Geospatial, Geophysical & Geotechnical Investigation of Glacial Depositions in Sikkim Himalayas

Sandeep Kumar Mondal[1], Hrik Chaudhury[1], Deepali Anand[1], Rishikesh Bharti[1,2], Abhishek Kumar[1,2] and Arindam Dey[1,2]

[1]Department of Civil Engineering, Indian Institute of Technology Guwahati, Assam-781039
[2]Center for Disaster Management and Research, Indian Institute of Technology Guwahati, Assam-781039

Correspondence to: Rishikesh Bharti (rbharti@iitg.ac.in)

Abstract

The glaciers in the Himalayan Cryosphere are predominantly covered with debris. Especially in the eastern Himalayan region, where slope failures are a serious concern and demand engineering insight. This study aims towards a comprehensive investigation of glacial deposits (moraine and lacustrine depositions) in the Sikkim Himalayas using an integrative geospatial-geophysical-geotechnical approach. The analysis includes assessing debris coverage, broadband albedo, glacial surface temperature (GST), and temporal variations in supraglacial inundation using satellite remote sensing techniques. The study indicates an increasing trend in supraglacial inundation since October 2014, suggesting the formation or expansion of supraglacial lakes/pools and an associated increase in the melt regime. Geophysical investigations using multi-channel analysis of surface waves (MASW) and ground-penetrating radar (GPR) have provided insights into stratigraphy and subsurface properties. Geotechnical investigations of glacial deposits collected from the Changme and Rathong glacial snouts have helped to understand their engineering and index properties. This is crucial for assessing the stability of slopes and natural embankments of glacial lakes. Analyzing the samples using field-emission scanning electron microscopy (FESEM) and X-ray diffraction (XRD) has provided insights into their microstructural morphology and mineral composition, respectively. Stability assessments using the limit equilibrium method (LEM) indicate that the moraine slopes have a high susceptibility to failure, with the factor of safety (FoS) ranging between 0.59 and 0.96 at different sections and profiles. Also, the presence of glacial calving zones exacerbates the risk of slope failure. Such detailed investigation is essential for understanding glaciology comprehensively and planning glacial hazard mitigation strategies in the Himalayas.

1. Introduction

The Himalayas, also termed “The Third Pole,” are categorized as the youngest but fragile mountain system on Earth. Being tectonically active and geologically complex, the Himalayan arc and its cryospheric environment have a direct influence on the regional hydrology and climate control of the subcontinent. Specifically, remotely located high-altitude glacial bodies, their dynamicity, melt regime, and associated natural hazards have gained paramount research momentum in the past few decades (Corripio et al. 2007; Gomez et al. 2022). Glaciers of the Himalayan cryosphere, especially located in the northeastern regions of the arc, are mostly debris-covered. The origination of debris coverage over a glacial body comprises various sources, which include local rock of the glacial region, ice falls, and/or wind-blown dust (Huo et al. 2021). Debris cover may also find its origin in meteorites, pollutants, microorganisms from sea spray, and volcanic eruptions (Cassidy et al. 1992; Hoover et al. 2001). However, the most predominant debris generation process is glacial erosion (Herman et al. 2021). Supraglacial debris influences the surficial melting of metamorphosed ice by acting as an insulating stratum (Nicholson 2005; Balaban et al. 2024). Where a thick blanket of debris over glacial ice insulates solar insolation, a thin debris coverage may result in more absorption of solar radiations thereby reducing the albedo (Li et al. 2013; Bozhinskiy et al. 1986). Thus, glacial debris and its properties, such as textural and lithological aspects, thickness, moisture content, and thermal properties, may alter the glacier-climate response mechanism in comparison to a clean or debris-free glacier (Racoviteanu et al. 2022).

Glaciers act as excellent indicators of climate change (Shrestha and Aryal 2011; Scherler et al. 2011; Bolibar et al. 2022). Studies reveal that the present-day Himalayan landscape is carved out as a result of multiple glacial and interglacial cycles of the Quaternary period (Garg et al. 2019; Shukla et al. 2019). Glaciers leave imprints on the land surface as depositional and erosional landforms, thereby revealing the driving factors for their recession and advance (Evans 2016; Singh et al. 2022). Some of the basic glacial landforms include supraglacial, lateral, and recessional moraine deposits, glacial till, and varved clays (Fredin et al. 2017; Clarke 2017). In this context, assessing the properties of glacial moraine deposits forms a starting point for understanding the physical and engineering aspects of glacial landforms. Especially in the case of the Sikkim Himalayas, where some of the moraine-dammed glacial lakes have expanded significantly in the past few years in terms of area and volume. Figure 1 shows a significant increase in the areal coverage of South Lhonak glacial lake (more than 1200%) since

1967. It is located at the western boundary of North Sikkim and was recently breached on 4th October 2023 (Zhang et al. 2024; Mondal et al. 2024). Such an increase in the areal coverage of a naturally-dammed glacial lake is attributed to a substantial increase in the lake volume, thereby increasing the vulnerability of the moraine dam. This necessitates the extensive investigation of glacial deposits, especially moraine and lacustrine deposits, in terms of their physical and engineering properties. However, because of various challenges in studying the Himalayas due to rugged topography, harsh weather conditions, and security constraints (Agarwal et al. 2019), there exists a knowledge gap regarding the geospatial, geotechnical, and geophysical properties of glacial deposits.

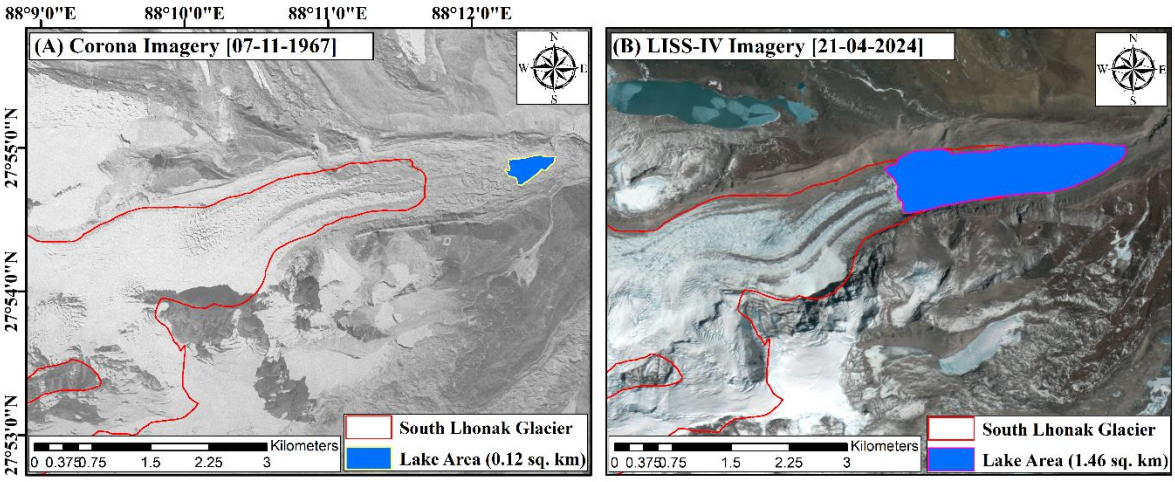

Figure 1: Map showing South Lhonak Glacial Lake as acquired from (A) Corona satellite in 1967 and (B) LISS-IV satellite in 2024 (post-GLOF)

With the advancement of geospatial technologies in the past few decades, continuous monitoring is now carried out in the inaccessible glacial environments of the Himalaya. Spaceborne and airborne remote sensing, geographical information system (GIS), global positioning system (GPS) and digital elevation models (DEMs) are effectively and frequently used to monitor, characterize and evaluate the glacial bodies and glacial landforms including velocity, mass balance, equilibrium line altitude (ELA), changes in length, area and surface of glaciers (Berthier et al. 2007; Singh et al. 2022; Mondal and Bharti 2023a). High-resolution optical satellite and airborne imagery have served in gathering much more accurate and detailed information about glaciers and glacial landforms up to much smaller scales (Veettil and Kamp 2017; Bertheir et al. 2023). Some of the recent studies confirm the effectiveness of high-resolution satellite datasets in the detailed monitoring of glacial landforms in the Himalayas (Donahue et al. 2023). However, their usefulness is hindered during monsoon periods due to obscuring cloud coverages. In this context, microwave remote sensing serves as an effective tool for investigating high-altitude glacial regions due to their cloud-penetrating capacities (Snehmani et al. 2015; Tanniru and Ramsankaran 2023; Mondal et al. 2023b).

Records of earthquakes (Mexico earthquake of 1985, Loma Pieta earthquake of 1989, Bhuj earthquake of 2001, etc.) and their extensive investigation prove that local site condition plays an influential role in the amplification of ground motions (Nath et al. 2018). The bedrock depth significantly alters the dynamics of the soil-subsurface system (Nath and Jakka 2012). Therefore, it is crucial to understand the subsurface as accurately as possible because of its immense implication on the analysis of seismic impacts (Bard 1995; Nath et al. 2015). The conventional techniques of subsurface geotechnical exploration have their challenges regarding extensive manpower and the cost involved. In this context, seismologists around the globe have begun to venture into some of the advanced geophysical techniques in exploring the subsurface and its geology. This results in easy and comparatively faster acquisition of data and processed information. Moreover, using geophysical techniques facilitates the investigation of a much larger area. Some of the areas where geophysical investigation finds wide application are exploration of fossil fuel, mineral exploration, detection of the subsurface water table, mapping permafrost, block field, sediment deposits underneath, internal structure, and depth of landslides (Hauck 2003; Israil and Pachauri 2003; Sass 2007; Pazzi et al. 2019). However, subsurface investigation through geophysical techniques demands experience and skill as factors such as dispersion and wave attenuation, mechanical properties of subsurface material, and various geological boundary conditions may introduce ambiguity to the data. Schrott and Saas (2008) recommend using two or multiple geophysical methods to deduce a strong conclusion from the investigation. Subsurface investigations through combining two or more geophysical techniques have been effectively accrued, especially for the Himalayan region (Pilecki et al. 2017; Nath et al. 2018). The Himalayan arc, being tectonically active and seismically prone, has produced enormous catastrophic earthquakes such as the 1978 Assam earthquake, the 1905 Kangra earthquake 1934 Nepal earthquake, the 1991 Uttarkashi earthquake, the

1999 Chamoli earthquake, and many more (Nath and Thingbaijam 2012; Sana and Nath 2017). Therefore, it is necessary to apprehend the local site conditions of Himalayan regions: qualitative and quantitative.

This study aims to carry out a comprehensive geospatial-geophysical-geotechnical investigation of the high-altitude Sikkim Himalayas to analyze the characteristics of glacial deposits (moraine and lacustrine deposits). The findings of this investigation can provide valuable insights into the engineering properties of glacial depositions, which is crucial for water resource management and the development of mitigation strategies for potential glacial hazards in the future.

2. Study Area

Sikkim Himalaya is characterized by a significant variation in altitude and topographic slope. Bordered by Nepal to the west, Tibet to the north, and Bhutan to the east, the Sikkim state of India stretches from approximately 27° 00′ 46″ N to 28° 07′ 48″ N latitude and 88° 00′ 58″ E to 88° 55′ 25″ E longitude, covering an area of around 7096 km^2. About 43% of its terrain is characterized by steep slopes and rugged landscapes, with elevations ranging from approximately 300 meters a.s.l (above sea level) to 8598 meters a.s.l (Garg et al. 2019). The state harbors several glaciers covering a total area of 677.93 km^2 (RGI V7.0), from which the important rivers, namely Teesta and Rangit originate. Sikkim is divided into four 5th-order basins: East Rathong, Changme Khangpu, Talung, and Zemu (Raina and Srivastava 2008; Garg et al. 2019). Moraine deposits surround these glaciers and glacial lakes (Raj et al. 2013; Aggarwal et al. 2017). Moraine deposits in the Himalayan region act as an embankment/dam material for naturally forming glacial lakes. Their strength and holding capacity control the stability of glacial lakes in terms of breach and outburst flood. Moreover, the region is seismically active (Zone-IV), which adds an extra risk factor to the stability of glacial lakes in terms of future hazards (Begam et al., 2018). Figure 2 shows the study area map showing the locations of geophysical investigations. Figure 3 shows the moraine and lacustrine deposits at the snout of Rathong Glacier.

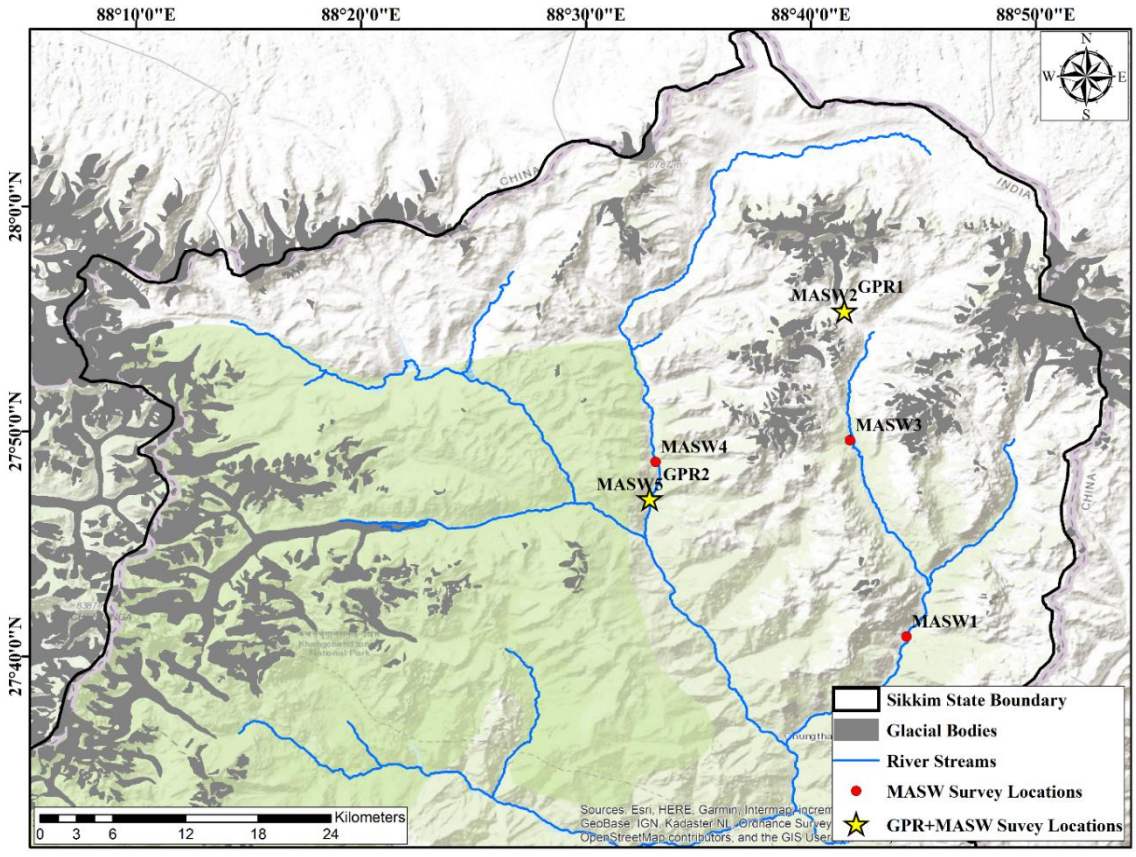

Figure 2: Study area map showing locations of field-based investigations

Figure 3: Photographs showing collection of moraine and lacustrine deposits from Rathong glacial snout

2.1. Glacial Geomorphology

Glacial bodies in the Sikkim Himalayas primarily consist of valley and cirque glaciers, with some hanging glaciers as well (Figure 4). Understanding the glacial depositions involves an analysis of the glacial geomorphology of the region. A glacial body can be described as a central mass of metamorphosed glacial ice with spreading arms or flanges. These flanges are mostly found at higher elevations, known as accumulation zones, and mainly consist of clean/debris-free glacial ice. In contrast, the main trunk of the glacier, which terminates at the glacial snout, is characterized by moraine and lacustrine deposits.

Valley and cirque glaciers in the area are separated by thin, jagged crests called arêtes, resembling serrated knives (Dubey et al. 2019). The low points along these crests are known as cols. In certain locations, triangular peaks called horns can be observed, formed by the erosion of multiple arêtes by the glacier. Moraine is a prominent feature of the glaciers in the Sikkim Himalayas as shown in Figure 5. As a glacier moves, it scrapes and collects rock fragments and soil from its surroundings, forming lateral moraines along its sides. These lateral moraines are preserved as high ridges on the glacier's surface. Terminal or end moraines are ridges of loose debris found at the snout of a glacier (Shrivastava et al. 2022). The size of these end moraines depends on whether the glacier is retreating, advancing, or in equilibrium. However, as a glacier retreats, postglacial erosion may eventually destroy the end moraine.

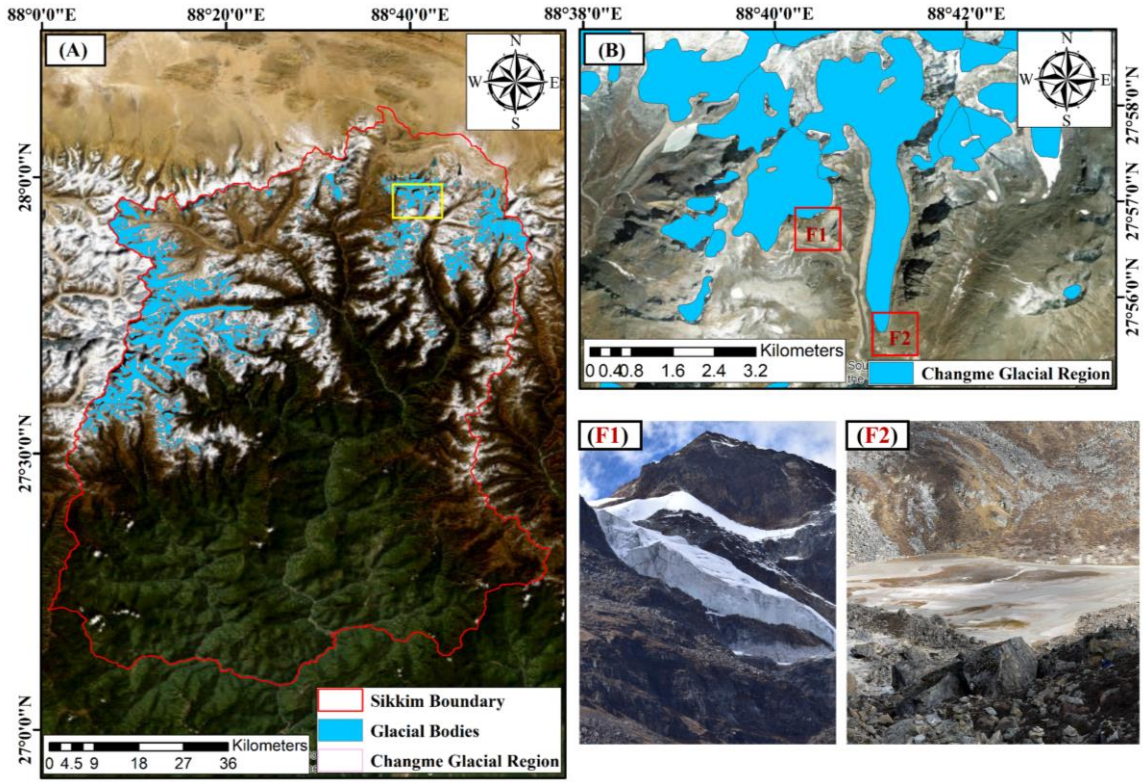

Figure 4: Map showing (A) Sikkim Himalayas, (B) Changme glacial region, field photographs of (F1) hanging glacial segment and (F2) lacustrine depositions at Changme glacial snout

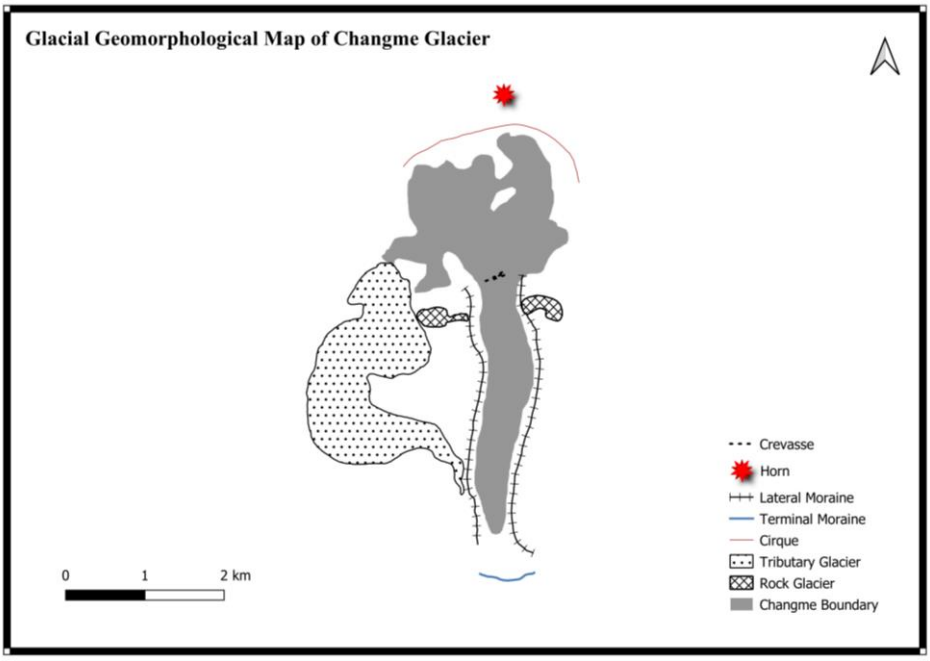

Figure 5: Glacial geomorphological map of Changme glacial region

Another important geomorphological feature of glaciers in the region is supraglacial lakes, which are temporary ponds of water found on the surface of the glacier. Some glaciers, such as the South Lhonak glacier, are connected to large moraine-dammed proglacial lakes (Figure 1). These lakes receive contributions from snow and glacial melt, making them more dynamic and causing an increase in their area over time. However, moraine-dammed proglacial lakes are considered more dangerous in terms of glacial lake outburst floods (GLOFs), making the stability assessment of glacial moraines crucial for the safety of these natural embankments.

3. Data and Methods

3.1. Datasets Used

In the proposed study, Landsat-8 (L8), Sentinel-1 (S1) C-band (5.405 GHz) synthetic aperture radar (SAR), LISS-IV (L4) onboard Reseoucesat-2 and Corona satellite imageries have been used. L8 satellite has two sensors: OLI (Operational Land Imager) with a spatial resolution of 30 meters composed of nine bands, and TIRS (Thermal Infrared Sensor) with a spatial resolution of 100 meters composed of a pair of bands (Claverie et al., 2018). It captures data at a temporal resolution of 16 days with a radiometric resolution of 16 bits. Each L8 scene covers an area of 185 km × 180 km. Datasets from L8 dated 10th Nov 2021, have been used to study glacial debris coverage, broadband albedo, and Glacial Surface Temperature (GST).

CORONA images, taken by KH-4A and KH-4B satellites, provide high-resolution imagery with ground resolutions of 1.83 m × 2.74 m, allowing detailed visualization of glacial features dating back to 1967 (Dashora et al. 2007). These historical images are crucial for analyzing changes in Himalayan glaciers over time. For analyzing glacial geomorphological features, imagery from the L4 (IRS-R2), dated 21st April 2024, has been used. The L4 sensor operates in two modes: mono and multi-spectral mode. In mono mode, data is collected in the red band with a swath of 70 km, while in multi-spectral mode, data is collected in three spectral bands (green, red, and near-infrared) with a narrower swath of 24 km (Verma et al. 2017). In this study, all three bands were used as false color composite (FCC) images for the analysis of glacial features and geomorphology. S1 Ground Range Detection (GRD) scenes, captured between 9th Oct 2014, and 28th April 2024, have been analyzed in Google Earth Engine (GEE) to extract backscatter information. Randolph glacial inventory (RGI V7.0) has been used for the glacial boundary information.

3.2. Geospatial Study

3.2.1. Debris Cover Mapping

Remote-sensing imagery stands out as the most effective tool for regularly monitoring glaciers, given the challenging and inaccessible terrain, as well as the harsh weather conditions common in high mountainous regions. Previous studies have documented the development and testing of various automated and semi-automatic remote-sensing techniques for accurately mapping clean glacier ice (Bhambri and Bolch, 2009; Paul et al., 2019). However, these methods prove ineffective when applied to debris-covered glaciers. This is because both supraglacial debris (debris covering the glacier surface) and periglacial debris (debris surrounding the glacier margin) exhibit a similar spectral response, as they originate from the same valley rock materials. In the present study, we opted for the band ratio proposed by Alifu et al. (2015) utilizing near-infrared (NIR), shortwave near-infrared (NIR), shortwave infrared (SWIR), infrared (SWIR), and thermal infrared (TIR) bands of Landsat-8 OLI dataset as mentioned in eq. (1):

$$Glacial\ Debris\ Index\ (GDI) = TIR\ \div (NIR\ \div SWIR) \quad (1)$$

Clean glacier ice exhibits high reflectivity in the visible to near-infrared wavelengths (0.4–1.2 μm) but very low reflectivity in the shortwave infrared (SWIR) wavelength region (1.4–2.5 μm). In contrast, supraglacial debris and other nearby non-glacier rocky surfaces have low reflectivity values in these wavelengths because they share similar spectral responses. In this regard, the thermal infrared (TIR) band can offer insights into temperature variations among different surfaces, aiding in the differentiation of supraglacial debris from other rock materials. Moreover, debris movies within the glacial body along with glacial ice. This movement of debris is towards the glacial terminus till it reaches a gentle slope which permits accumulation. Thus, topographic gradient of the glaciated terrain can be utilized to eliminate supraglacial debris from surrounding valley walls. In the present debris mapping, we have utilized slope threshold of <12° to segregate glacial debris from clean glacial ice.

3.2.2. Broadband Albedo

Albedo (α), also known as bi-hemispherical reflectance, is defined as the ratio of the radiant flux reflected from a unit surface area into the entire hemisphere to the incident radiant flux of hemispherical angular extent within the visible, near-infrared (NIR), and shortwave infrared (SWIR) regions of the electromagnetic spectrum (0.3 - 2.5 μm). Albedo plays a crucial role in energy budget studies and glacial health monitoring, particularly in high-altitude Himalayan regions where it tends to be high due to the extensive coverage of snow and ice. Any deviations from these high albedo values can significantly impact surface mass balance and melt patterns.

Traditionally, albedo data were obtained using instruments mounted on automatic weather stations (AWSs) at hourly or sub-hourly temporal resolutions. However, while these point measurements can provide continuous albedo data for specific locations, they may not represent an entire glacier. In this context, multispectral satellite remote-sensing datasets prove to be extremely valuable. In our study, we utilized the algorithm proposed by Liang

(2001) on the Landsat-8 OLI dataset to calculate the broadband albedo of glacier areas within the Sikkim Himalayas as mentioned in eq. (2).

$$Broad\ band\ Albedo\ (\alpha) = 0.356Ref_{B2} + 0.130Ref_{B4} + 0.373Ref_{B5} + 0.085Ref_{B6} + 0.072Ref_{B7} - 0.0018 \quad (2)$$

where *Ref* indicates the reflectance of each band. One key benefit of this algorithm is its ability to incorporate contributions from a broader spectrum range compared to others (Traversa et al. 2021). This enables it to detect albedo variations resulting from changes in grain size, which notably affect near-infrared and shortwave infrared wavelengths.

3.2.3. Glacial Surface Temperature

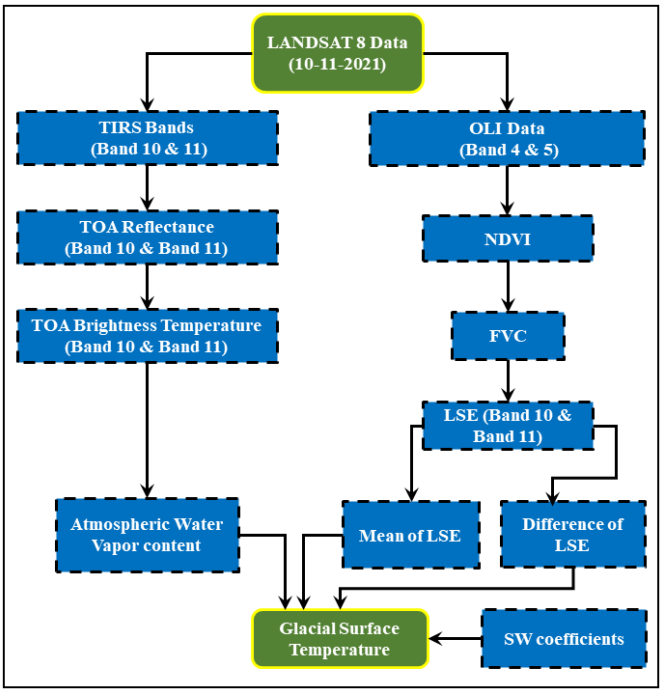

Figure 6: Systematic flow diagram to estimate glacial surface temperature (GST) using split-window algorithm

Glacial surface temperature (GST) is influenced by both atmospheric energy flux and the thermal dynamics at the interfaces of ice, water, and debris (Liao et al. 2020). Understanding the surface temperature of glaciers is essential for assessing their accumulation or ablation state, making GST an important indicator of glacial health. In this study, we utilized Landsat-8 OLI and TIRS (Thermal Infrared Sensor) bands through a split-window (SW) algorithm to estimate GST. Figure 6 illustrates the schematic representation of GST estimation using the SW algorithm. The process begins with estimating the Top of Atmospheric (TOA) spectral radiance (L_λ) from the thermal bands (Band 10 and 11). This radiance is then used to calculate the brightness temperature (BT), which represents the microwave radiation radiance propagating upward from the top of Earth's atmosphere. The next step involves computing the Land Surface Emissivity (LSE), which is a crucial parameter for GST derivation. Finally, the Land Surface Temperature (LST) is calculated using the structured mathematical algorithm, the Split-Window (SW) algorithm (Mondal and Bharti 2021).

3.2.4. Supraglacial Inundation

In the Google Earth Engine (GEE) platform, preprocessed S1 radar information is available. To calculate the backscatter coefficient (in dB) for each pixel from GRD data, several preprocessing steps were followed. These steps include applying precise orbit information, removing border and thermal noise, and performing radiometric calibration and ortho-rectification which were executed by Google as per the protocols of S1 toolbox software (Google Earth Engine 2022). The steps, such as incidence angle normalization and speckle filtering, were applied using GEE, as shown in Figure 7.

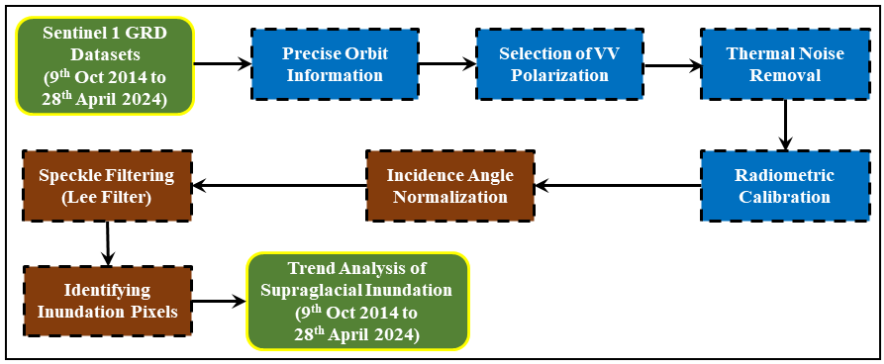

Figure 7: Systematic flow diagram to estimate temporal fluctuations in supraglacial inundation

For S1 time-series data, backscatter normalization is crucial (Weiß 2018). Backscatter values from the same area can vary based on the incidence angle, with smaller incidence angles resulting in higher backscatter values. Additionally, variations in incidence angles can occur within a sensor due to different acquisition geometries, tracks, or orbits (Gulácsi and Kovács 2020). This study applied the cosine correction method to normalize the backscatter values based on the ellipsoidal incidence angles (Hird et al. 2017). The next step involved speckle filtering. This is performed to substantially reduce granular image noise (speckle) caused by the interference of transmitted and received microwaves at the radar antenna (Lee et al. 1981; Gulácsi and Kovács 2020).

Finally, supraglacial melt-water pools were identified by visually interpreting high-resolution L4 imagery. Empirical threshold limits for backscatter values were established: pixels with values generally at or below -16 dB (for VV polarization) were considered to represent supraglacial water/inundation.

3.3. Geophysical Study

There are numerous geotechnical tests to understand the subsurface soil characteristics of a site. A standard penetration test (SPT) and cone penetration test (CPT) are the most commonly used field-based tests. Cyclic triaxial test, uniaxial compressive test (UCT), direct shear test (DST), and vane shear test (VST) are the most widely performed geotechnical tests in the laboratory. Both categories of tests have their advantages and disadvantages. Where the advantages of field-based experiments involve testing undisturbed samples in their natural environment and stratigraphic profiling, the disadvantages of such experiments include indirect and empirical measurement of engineering properties of soil, being labor-intensive, and involving colossal capital. Henceforth, engineers came up with the alternative of geophysical tests. A shock is created in geophysical methods like seismic reflection surveys or seismic refraction surveys. The reaction that the ground gives against the shockwave characterizes the subsurface soil properties.

The shear stiffness of soil is one of the most important properties engineers evaluate. The shear stiffness of soil can be interpreted with the response of ground to shear wave propagation, which is a body wave. Body waves have a very low signal-to-noise (SNR) ratio near the ground surface (Kramer 1996). So, Rayleigh waves are used to characterize soil properties of the top 50 meters of the ground. Rayleigh waves typically have elliptical motions and high SNR because of their low frequency, low shear, and high amplitude (Park et al. 1999). Moreover, Rayleigh waves have a velocity of nearly about 90 percent of that of the shear wave velocity. Multichannel Analysis of Surface Waves (MASW) is one of the most popular geophysical methods in practice these days. For imaging and describing the shallow subsurface, Rayleigh-type surface waves' frequency-dependent characteristics are used in this method for imaging and describing the shallow subsurface. In multichannel recordings, noise can be effectively identified and isolated based on unique trace-to-trace coherency in arrival time and amplitude (Park et al. 2007).

3.3.1. Multi-Channel Analysis of Surface Waves

Multi-Channel Surface Wave Analysis (MASW) is one of the most used geophysical methods to evaluate soil stiffness in the current practice. The non-invasive nature of the MASW method makes it the foremost choice for engineers to use for field exploration. The field instrument setup for this method consists of a hammer, a baseplate, multiple numbers of geophones, a triggering cable, control unit cables, a battery, and one data acquisition system, as shown in Figure 3 below. MASW survey can be done in both active and passive ways. In the field for active MASW survey, the base plate is placed at the start of the setup. One triggering geophone is placed just next to the baseplate. The triggering geophone is connected to a cable that bridges the Data Acquisition System (DAS) and the triggering geophone. Following the triggering geophone, multiple geophones are placed and connected through a cable to the DAS. This entire setup is shown in Figure 4 below. The base plate is struck with a hammer

to generate seismic waves. These waves are then captured through the geophones. The ground stiffness is evaluated based on the arrival time of seismic waves to each geophone. The ground stiffness profile with respect to depth is obtained at the middle of the setup in a static linear array. This is called the 1-D MASW survey. In the 2-D survey, the array is shifted parallelly through a certain distance. Multiple shifts provide the complete 2-D profile of ground stiffness with respect to depth. In the 3-D survey, a parallel shift, and a perpendicular shift are performed to generate a 3-D profile. MASW survey is also done passively, where the seismic waves captured are not generated with the hammer's strike. Instead, the waves produced from traffic, machines, blasting, etc., in the vicinity are used. The raw data of MASW provides dispersion curves. This dispersion curve is the phase velocity-frequency graph. This graph is derived from the Fourier transformation of the group velocity-frequency of the seismic waves captured through geophones. An inversion analysis is done on the dispersion curve to evaluate the subsurface's final shear wave velocity profile.

Figure 8: Photographs of MASW components (left) and field installation (right)

Records of the multichannel surface waves have been acquired during a field investigation conducted between 15th and 24th Oct 2021 in the North Sikkim region. The datasets have been collected at different locations and altitudes along with the Changme glacial snout consisting of relatively homogenous glaciofluvial deposits, as shown in Figures 5 and 8. The surface wave records have been collected using two different configurations of vertical geophones (12/24) arranged as a linear array with a 4.5 Hz natural frequency. Various combinations for measurement profiles and source offsets have been used, as shown in Table 1. For every combination, multiple surface wave records have been acquired, thus resulting in 167 records. The impact load has been created using a sledgehammer (10 Kg). The notion behind acquiring a large volume of datasets using multiple configurations of measurement profiles lies in the appropriate choice for the most informative results through the proposed methodology.

Table 1: MASW configurations (bold and underlined values are for the results presented)

Survey Code	Location	Configuration Orientation	Altitude (m a.s.l)	Number of Geophones	Offset (m)	Geophone Interval (m)	No. of Data
MASW1	Lachung Playground	NE-SW	2585	**24**	**3**,4	**1**	11
MASW2	Changme Glacial Snout	N-S	4698	**24**	**1**,3	**1**	14
MASW3	Yumthang Valley	N-S	3693	12	1,3	2	12
				24	**1**,3	**1**	13
MASW4	b/w Lachen & Thangu Valley	N-S	3268	12	1,3	2	14
				24	1,**3**	**1**	16
MASW5	b/w Lachen & Thangu Valley	N-S	3117	12	1,2,3,4	2	21
				24	**1**,2,3,4	**1**	23
		E-W		12	1,2,3,4	2	20
				24	1,2,3,4,	1	23

3.3.2. Ground Penetrating Radar

GPR is a non-destructive and non-invasive geophysical tool extensively used for subsurface investigations through imaging. Imaging the subsurface at shallow depths (≤10 m) can be performed at high resolution. For investigating much deeper depths, the resolution and accuracy get compromised. GPR operates according to the concept of dielectric constant. As moving vertically downwards on a ground surface, the properties of the soil layers change in terms of dielectric constants. The lower dielectric constant of soil indicates higher electromagnetic (EM) wave velocity and vice versa. The frequency of the antennas used in GPR range from 4 GHz to 10 MHz. The penetrating depth of the transmitted EM waves is a function of the antenna frequency. The instrument can be used in two different modes: transmission or frequency mode. The most commonly used method is the reflection profiling survey, performed using two antennae with a separate receiver and transmitter and is therefore also termed as bi-static mode. The antennas are positioned directly on the ground surface or near the ground. To enhance the speed of the survey and protect the equipment from damage, the antennas can be mounted on a wheeled platform or sled/trolley.

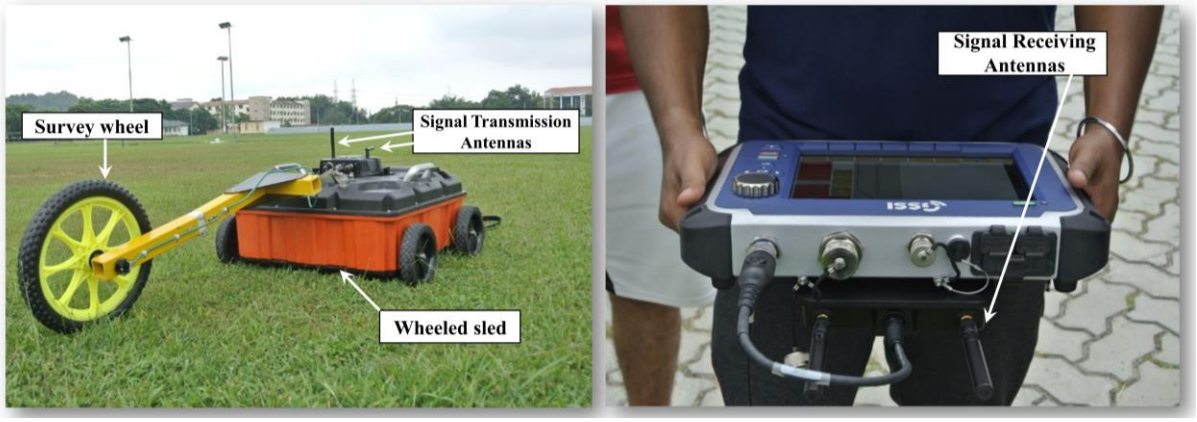

Figure 9: Photographs of GPR components (left) and the control unit (right)

An investigation conducted by Bristow and Jol. (2003) shows that using 100 MHz antennas results in the best trade-off between the resolution of data acquisition and the penetration depth. However, lower-frequency antennas (35 and 80 MHz) can be used to investigate bedrock at much deeper depths. Sass (2007) extensively measured the sediment thickness and depths of alpine talus slopes using GPR, seismic refraction, and 2-D resistivity survey. It has been observed that utilizing two or multiple geophysical techniques improves the quality of data interpretation. GPR's resolution and range primarily depend on the antenna frequency and sediment mineralogy (Motoyuki 2001). The major limitation of GPR is its incapability to determine the subsurface geology's mechanical or index properties. The moisture content of the subsurface layers profoundly influences the penetration depth of EM waves as soil's conductivity and electrical resistivity change. In the present study, a wheeled trolley-mounted GPR (200 MHz) has been used, having six major hardware components: (a) control unit, (b) transmitter, (c) receiver, (d) antennae, (e) survey wheel, (f) interface, display, and data storage module (Figure 6 and 7). Automatic gain control (AGC) was applied while acquiring data (Neal, 2004). The datasets have been collected through point-to-point and time modes of the survey. Further, processing of the datasets has been performed using the GPR manual supplied by the Geophysical Survey System instruments (GSSI) in the RADAN (GSSI computer-based interface) software applying 2-D spatial fast Fourier transform, finite impulse response (FIR), and infinite impulse response (IIR) filters, gain control, de-convolution, surface normalization, hyperbola migration, and bandpass filtering.

3.4. Geotechnical Study

Moraine and lacustrine samples collected from the Changme and Rathong glacial snouts were tested for their geotechnical properties in the geotechnical laboratory, Department of Civil Engineering, Indian Institute of Technology Guwahati. The samples were tested for relevant index and engineering properties as per the provisions of the Indian Standard (IS) codes (IS 2720 (Part III) – 1980; IS 2720 (Part IV) – 1985; IS 2720 (Part V) – 1985; IS 2720 (Part VI) – 1972; IS 2720 (Part XIII) – 1986; IS 2720 (Part XVII) – 1986). Moreover, to conduct the micro-structural characterization and understand the mineralogical composition of the samples, Field emission scanning electron microscopy (FESEM), X-ray powder diffraction (XRD) and energy dispersive X-ray analysis (EDX) was performed.

3.4.1. Mechanism of Glacial Moraine Slopes

The mechanism of slope failures in the Himalayan region is influenced by a combination of factors, including slope geometry, material properties, pore pressure, stress state, slope structure, and boundary conditions. The

geometry of the slope is closely linked to the volume of displaced material, failure type, and critical failure surface. Glacial moraine slopes consist of highly fragmented rocks mixed with coarse to fine sediments. The moraine slopes examined are naturally deposited in the Changme and Rathong glacial snout regions. Figure 10 shows the slope profiles on either side of the glacial snouts, derived using 12.5m terrain-corrected ALOS PALSAR DEM.

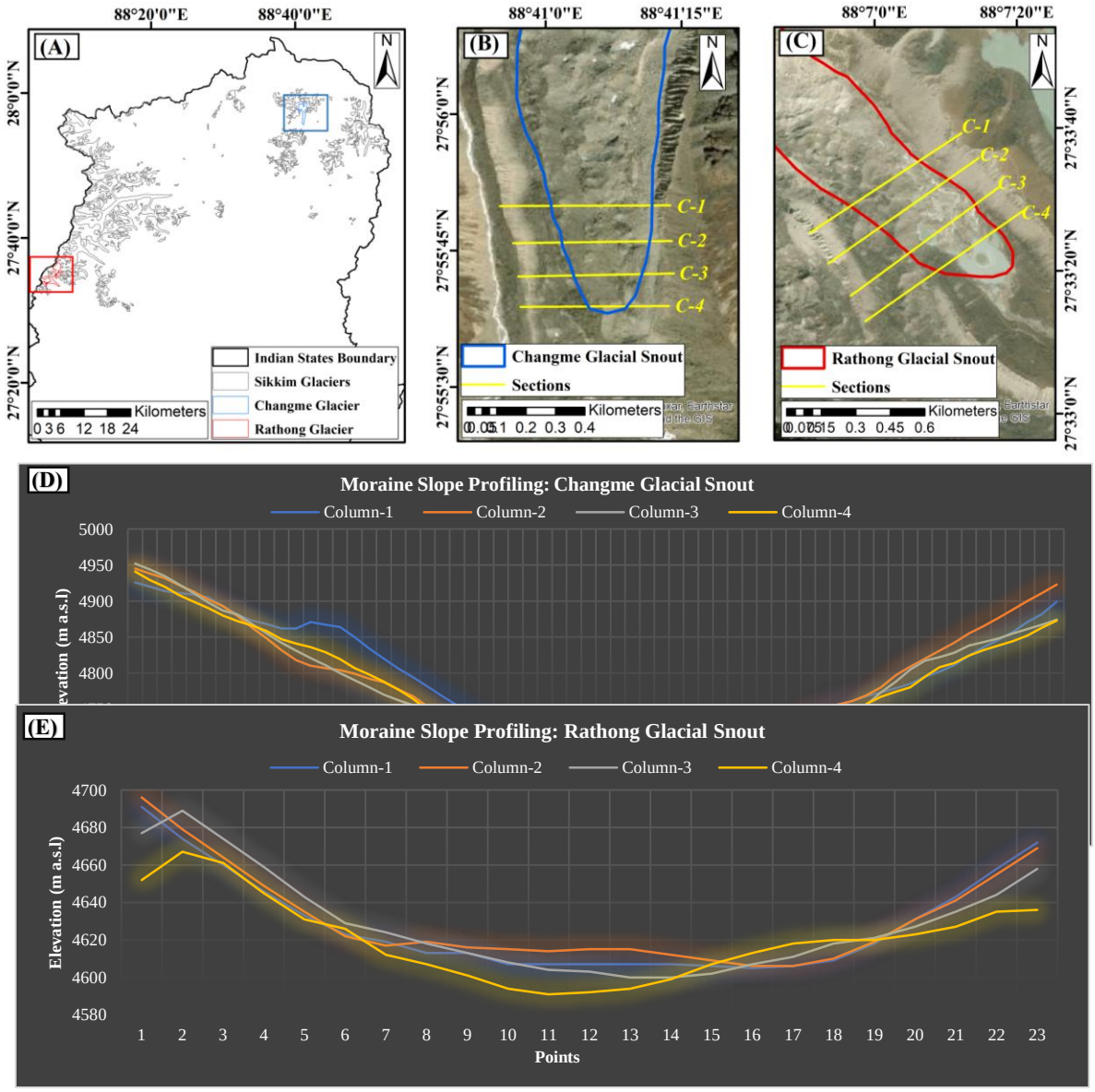

Figure 10: Map showing (A) Sikkim glaciers, moraine slope sections (C-1/C-2/C-3/C-4) at (B) Changme glacial snout and (C) Rathong glacial snout, followed by (D) slope profiles on the left and right side of Changme glacial snout and (E) Rathong glacial snout

The limit equilibrium method (LEM) remains the most widely used and acknowledged approach for slope stability analysis due to its versatility and simplicity (Abramson et al. 2001; Behera et al. 2016). Numerical methods for assessing slope stability can be time-consuming and have practical limitations in some scenarios. In contrast, LEM can still provide reliable and accurate results for most homogeneous materials (Cheng et al. 2007). Numerical methods like the finite element method (FEM) generate a unique failure surface, making it difficult to define other potential failure surfaces. In contrast, LEM can identify two or more critical failure surfaces with similar factors of safety (FoS) that should be taken into account in stabilization measures. Consequently, numerical methods might highlight a less significant local slip surface while overlooking a more critical failure surface. Thus, the LEM is a more effective tool for analyzing soil slope stability (Cheng et al. 2007; Singh et al. 2018). In this study, forward deterministic LEM has been used to compute the stability of naturally-deposited moraine slopes on either side of Rathong and Changme glacial snouts using Slide v7.0, a commercial software from Rocscience. For calculating the FoS, the current study employs the Bishop Simplified (BS), Janbu Simplified (JS), Corps of Engineers (CoE), and Morgenstern–Price (MP) methods.

4. Results and Discussion

4.1. Monitoring glacial properties

Glaciers serve as crucial indicators of climate change. Satellite remote sensing is vital in monitoring their properties over extensive spatial scales and extended time periods. By providing data on glacial dynamics, including glacial surface temperature (GST), broadband albedo, and debris coverage, remote sensing enables researchers to understand better how glaciers respond to environmental changes. Moreover, monitoring changes in glacial properties using remote sensing helps identify areas at risk of glacial-related hazards such as glacial lake outburst floods (GLOFs) and debris flows, allowing for better hazard assessment and mitigation strategies.

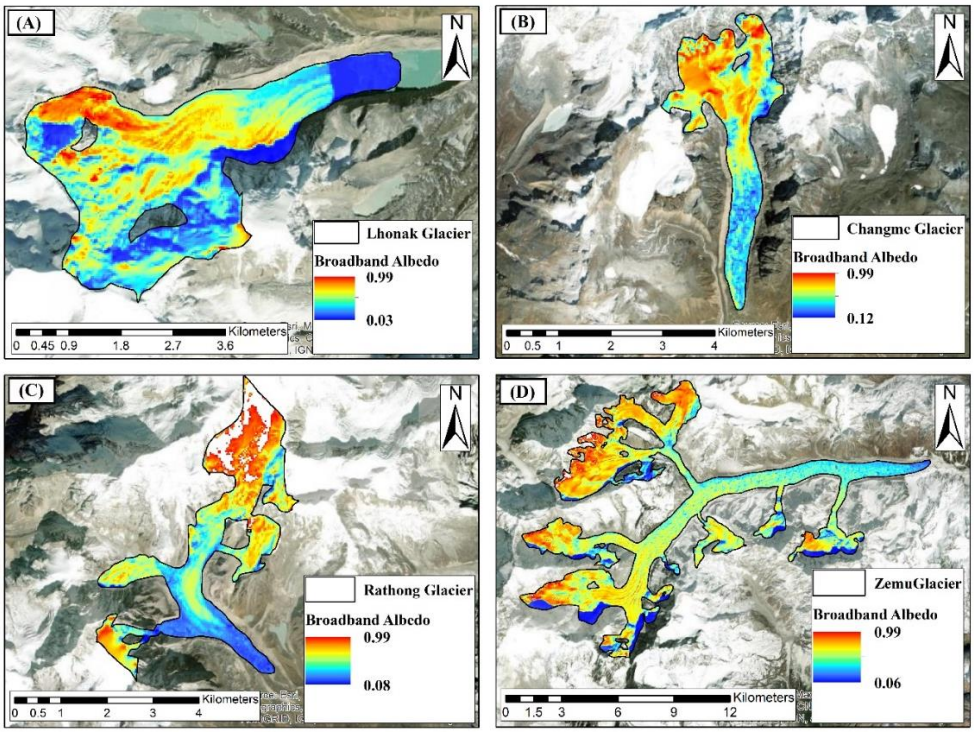

Figure 11: Broadband Albedo of (A) South Lhonak glacier, (B) Changme glacier, (C) Rathong glacier and (D) Zemu glacier

We examined the glacial bodies for their reflective (albedo), emissive (GST), compositional (debris cover), and backscatter response (Supraglacial lakes) properties. Utilizing the glacial database from the Randolph Glacial Inventory (RGI V7.0), we monitored 106 glacial bodies for their albedo, LST, and debris cover. Figure 11 shows the broadband albedo of some of the major glaciers of the Sikkim Himalayas, namely- South Lhonak Glacier, Changme Glacier, East Rathong Glacier, and Zemu Glacier. The areal coverage of these glaciers is 11.71 km^2, 4.85 Km^2, 8.29 Km^2, and 68.67 Km^2, respectively. Higher albedo corresponds to clean snow/glacial ice and can be observed at the higher reaches of the glacial body. As moving towards the glacial snout, the albedo falls due to increased dominance of glacial debris/moraine. Minimum albedo values are observed within some patches of glacial edges due to shadow effects. Figure 11A shows a large area at the snout of South Lhonak glacier with minimum albedo due to the presence of a proglacial lake. Water absorbs a large amount of incident solar radiations in the visible, NIR, and SWIR regions of the EM spectrum, and therefore, the albedo falls in the case of glacial lakes. Such observations can also be made within the main trunk of the glacial bodies due to the presence of supraglacial lakes/pools.

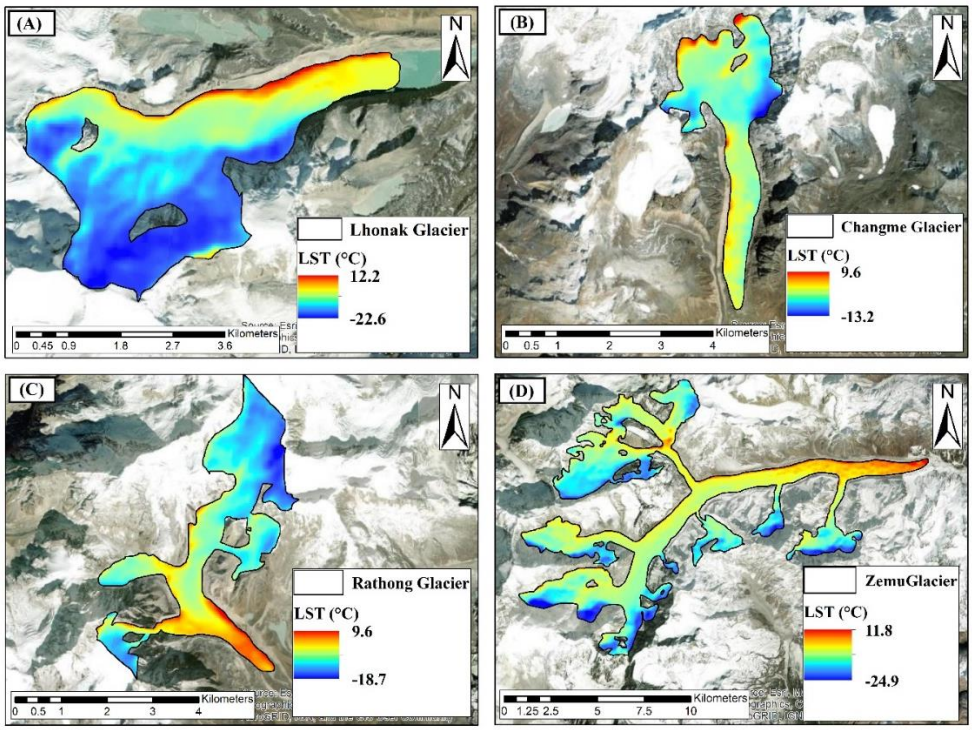

Figure 12: Glacial surface temperature (GST) of (A) South Lhonak glacier, (B) Changme glacier, (C) Rathong glacier and (D) Zemu glacier

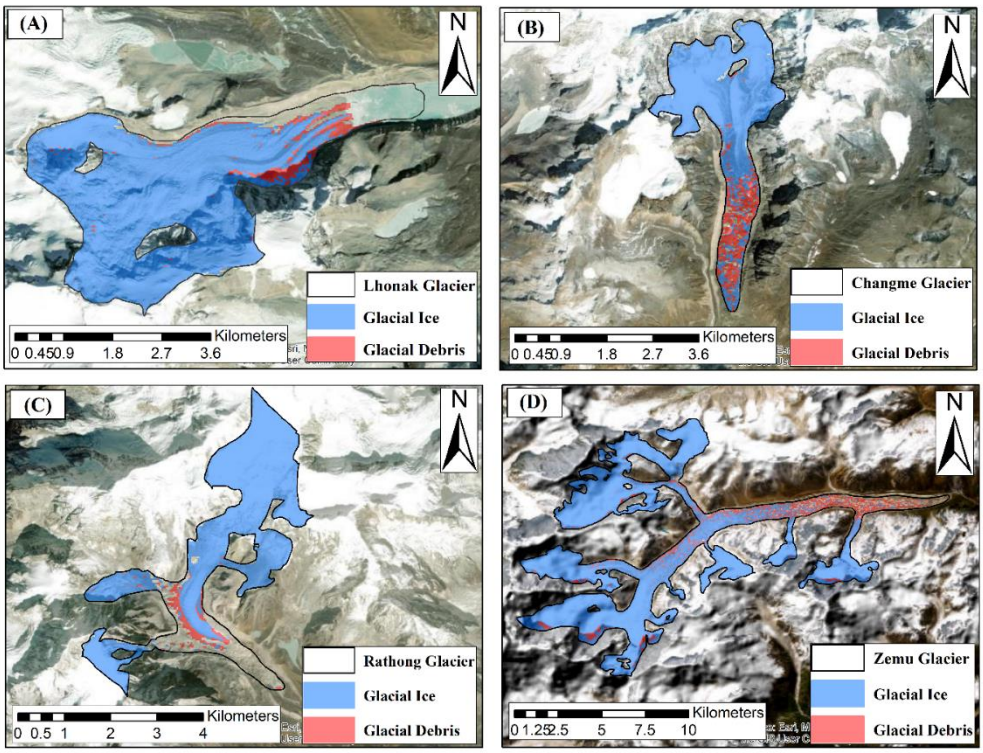

Figure 13: Glacial debris map of (A) South Lhonak glacier, (B) Changme glacier, (C) Rathong glacier and (D) Zemu glacier

Figure 12 shows the surface temperature within glacial bodies that corroborate with the observed albedo. The lowest values of GST are observed at the higher reaches of the glacial bodies where maximum albedo is captured. As higher albedo values indicate more broadband reflectance, thus less solar radiation is absorbed by the glacial ice resulting in reduced GST. On the other hand, the lower reaches of the glaciers, especially within the main trunk

(due to medial moraine) and glacial snout (due to lateral and terminal moraine) are observed with much higher values of GST. Glacial debris/moraine results in more absorption of solar radiations thus less albedo and more GST. In order to confirm the observations, glacial debris mapping is performed (Figure 13). It can be clearly observed that the higher reaches of the glaciers are mostly composed of clean glacial ice/snow. Whereas the glacial trunk and snout regions are moistly covered by glacial debris where maximum GST and minimum albedo is observed. Figure 13 shows the South Lhonak, Changme, Rathong, and Zemu glaciers with glacial debris coverage of 5.9%, 18.9%, 5.1%, and 10.3%, respectively. This can be attributed to the melting regime of the glaciers within the Sikkim Himalayas. Glacial debris/moraine can result in enhanced melting of glacial ice within the main trunk and glacial snout. Melting of glacial ice can be reflected as increased areal coverage of glacial lakes (supraglacial and proglacial lakes).

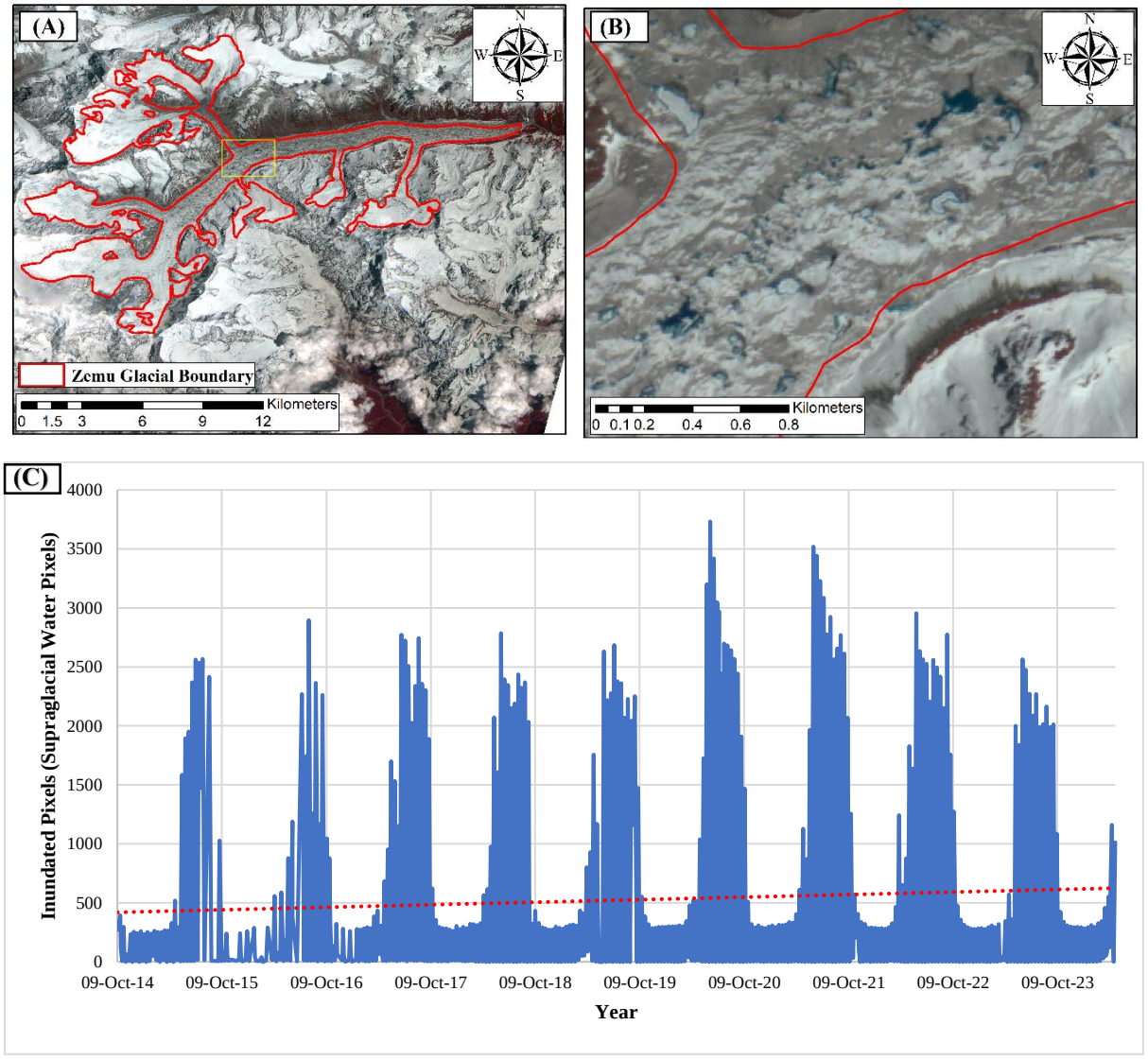

Figure 14: False Color Composite (FCC) Map showing (A) Zemu glacier, (B) section of glacial trunk showing supraglacial lakes/pools, and (C) temporal fluctuations in supraglacial water pixels

Figures 14A and 14B show the Zemu glacial body and a section of the glacial trunk with supraglacial lakes (blue in FCC). Figure 14C represents the temporal variations in the number of pixels indicated as water (supraglacial pixels) within the Zemu glacial body. There is a rising and falling trend in the number of inundated pixels (water) every year which indicates seasonal variability. During winters (Nov-April), supraglacial lakes remain in a frozen state, due to which the C-band backscatter-based count of inundation pixels reduces. However, with the end of the winter season, this number increases significantly, showing a maximum number of inundation pixels in July and August that starts falling afterward. Such periodicity continues every year. However, a significant increase in the inundation pixels has been observed in the past few years (2020, 2021, and 2022), indicating an increase in the count of water pixels, thereby increasing in supraglacial lakes (area and/or count). It is important to note that such observations on the variations of supraglacial water pixels are challenging to execute with the help of optical

satellite imagery due to obscuring cloud coverages. Such observations can be connected with enhanced glacial melting in the recent past years which resulted in the increase of the areal coverage and/or number of supraglacial lakes. Similar observations have been made in the case of the other glacial bodies of the Sikkim Himalayas, such as the South Lhonak Glacier (Figure S1), Changme Glacier (Figure S2), and Rathong Glacier (Figure S3).

Therefore, health monitoring of the glacial bodies helped identify potential glaciers for field- and lab-based investigations. Based on the accessibility, topographic feasibility (for geophysical investigation), and extensive geomorphological investigations, we selected Changme and Rathong glaciers as the best possible glacial bodies for the geophysical and geotechnical investigations.

4.2. MASW Survey and Dispersion Analysis

Figure 15: MASW survey at a location (MASW5) between Lachen and Thangu Valley (left) and (MASW2) Changme glacial snout (right)

The first step is dispersion analysis. The main objective behind dispersion analysis is identifying experimental dispersion curves based on the MASW records. For active-source surveys, the transform-based approach is most commonly used (Socco et al. 2010). This involves the phase shift method (Park et al. 1998), slowness-frequency transform (McMechan and Yedlin 1981), and frequency-wave number transform (Yilmaz and Baysal 2015), where the transformation of the multichannel time series is performed into a different domain from space-time domain. The phase shift method is comparatively more computationally efficient and robust, providing fundamental mode phase velocities more accurately even when the datasets are acquired from a limited number of geophones. The phase shift method has three main steps: amplitude normalization and Fourier transformation, dispersion imaging, and extraction of dispersion curves. In the present study, the surface wave records have been analyzed using a phase shift approach in SURFSEIS 6.0 software, as shown in Figure 16.

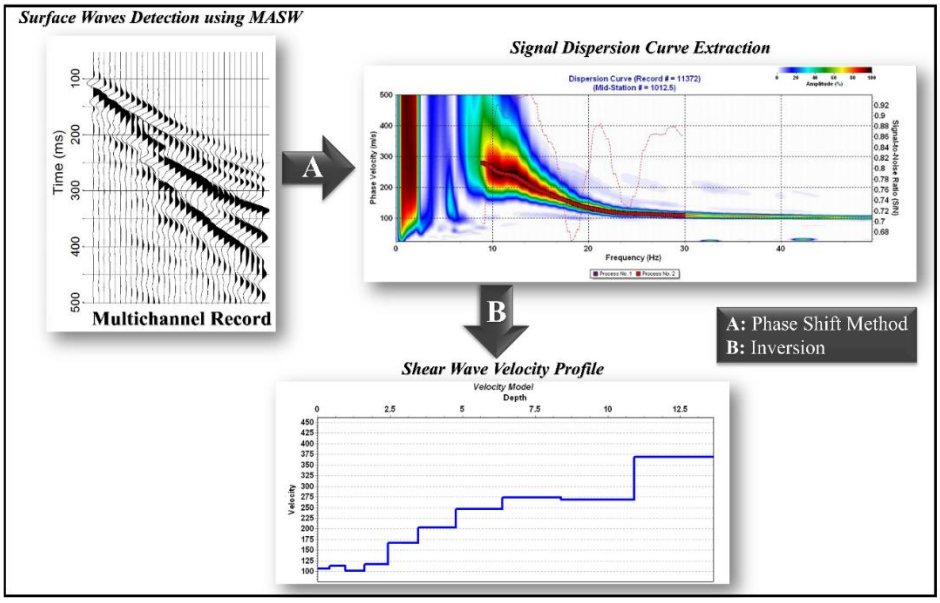

Figure 16: Flow diagram for MASW data processing

Every record has been processed separately using the phase shift approach. The variability associated with the identified elementary dispersion curves has been subsequently evaluated through the coefficient of variation (C_V) at each frequency among the values of estimated phase velocity (eq. 3), where S_c corresponds to the standard deviation and $\bar{c}$ is the mean phase velocity values at frequency *f*.

$$C_V = \frac{S_c}{\bar{c}} \tag{3}$$

The best-obtained records of dispersion images, along with the fundamental mode dispersion curves acquired for five locations in North Sikkim with the best-suited measurement profile configuration, have been shown in Figures 17 to 21. The estimates for the dispersion curve as obtained from diverse measurement profile configurations are reliable, characterized by the coefficient of variation (C_V) ranging between 1-8% at each frequency. The higher frequency components portray less variability than the lower frequency components.

The configuration adopted for the measurement profile, i.e., the source offset and the receiver length spread, resulted in significant effects on the obtained dispersion imagery and, subsequently, on the dispersion curve frequency range. The recorded time series obtained from the shortest receiver spread provided the most information on dispersion properties of higher frequency (shorter wavelength) wave components propagating through the uppermost soil layers. Increasing the length of receiver spread resulted in enhanced spectral resolution facilitating the identification of fundamental mode at the lower frequencies. Therefore, it has been observed that a longer receiver spread resulted in greater investigation depth as per the existing recommendations (Park et al., 2010).

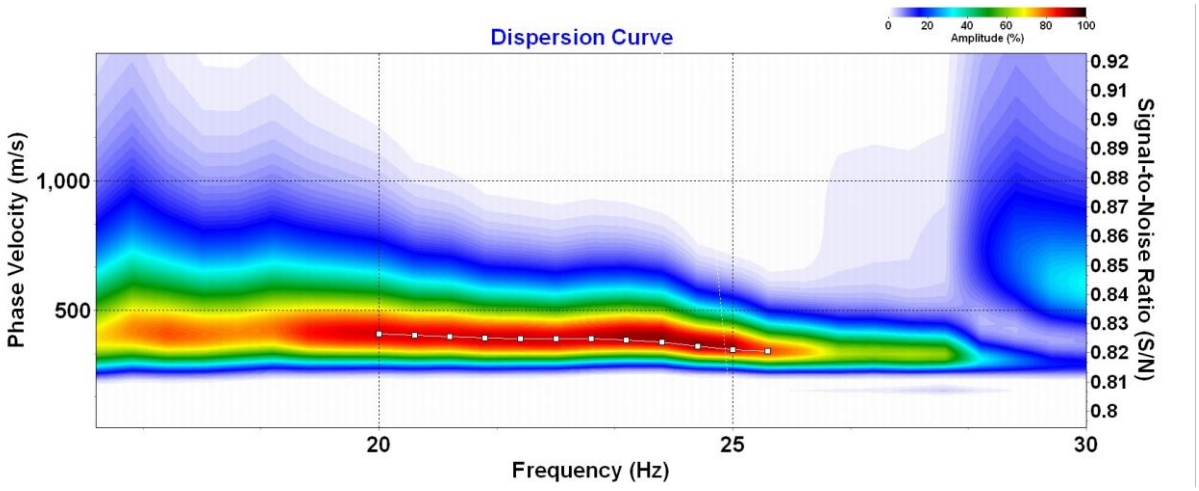

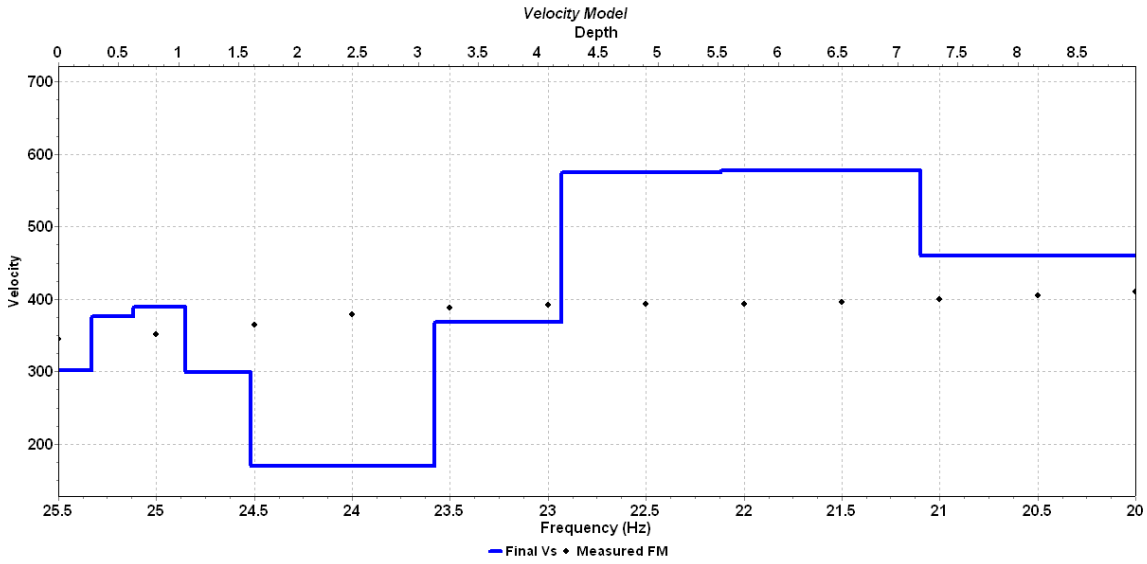

Figure 17: The fundamental-mode dispersion curve and shear wave velocity profile at Lachung playground (MASW1)

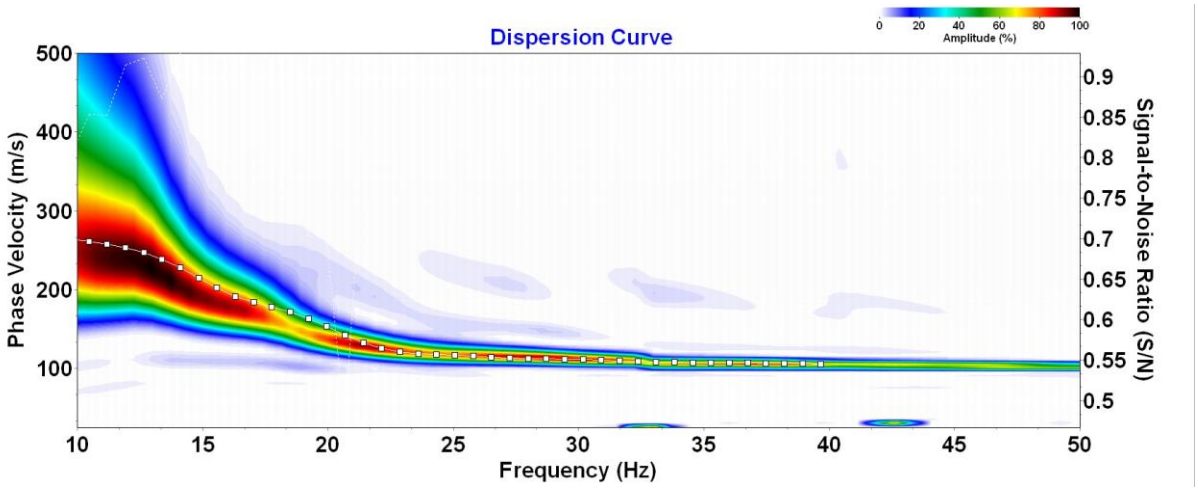

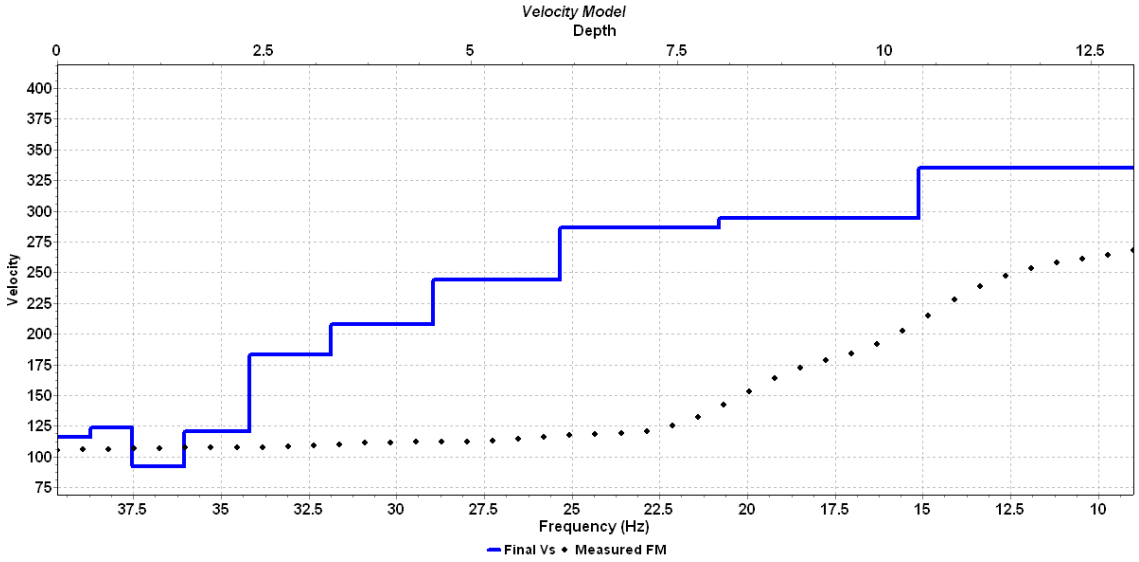

Figure 18: The fundamental-mode dispersion curve and shear wave velocity profile at Changme glacial snout (MASW2)

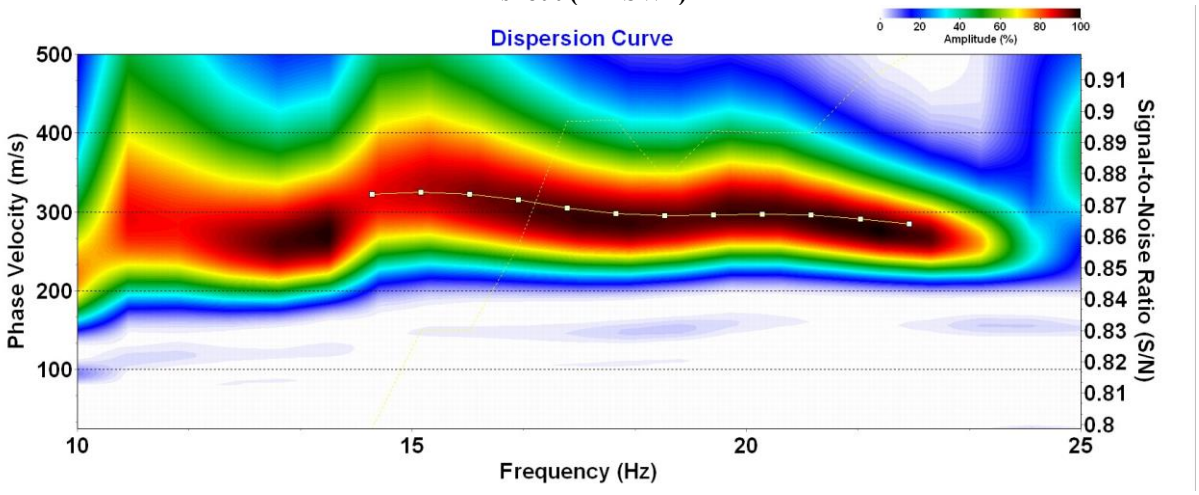

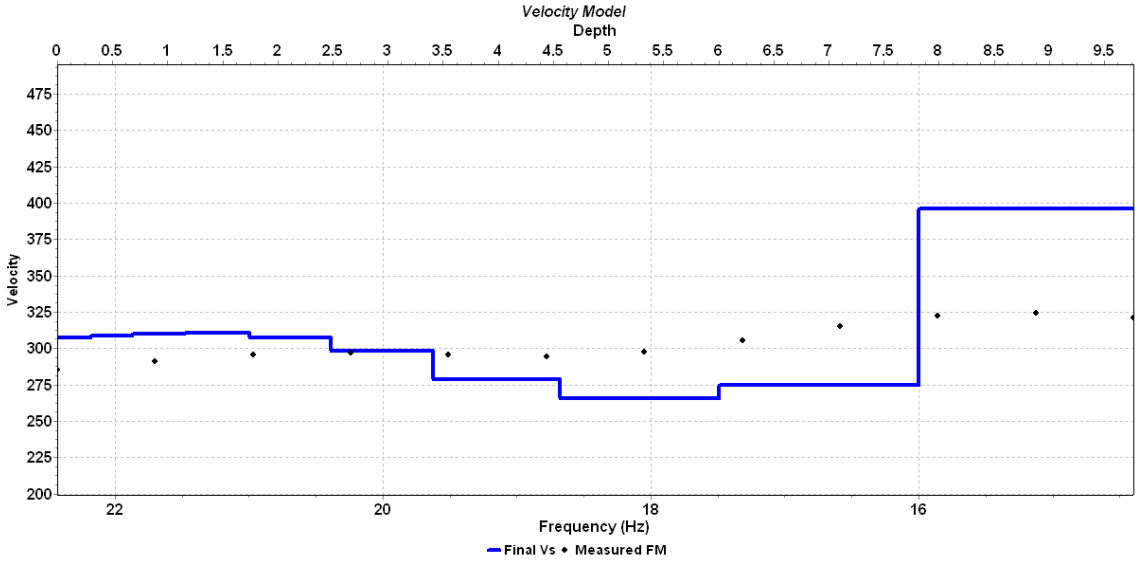

Figure 19: The fundamental-mode dispersion curve and shear wave velocity profile at Yumthang valley (MASW3)

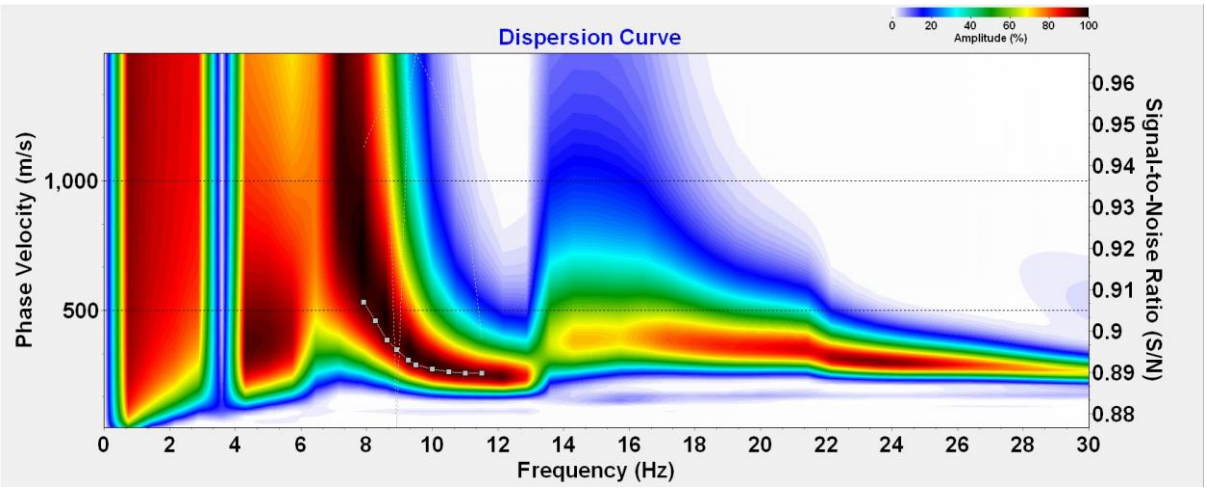

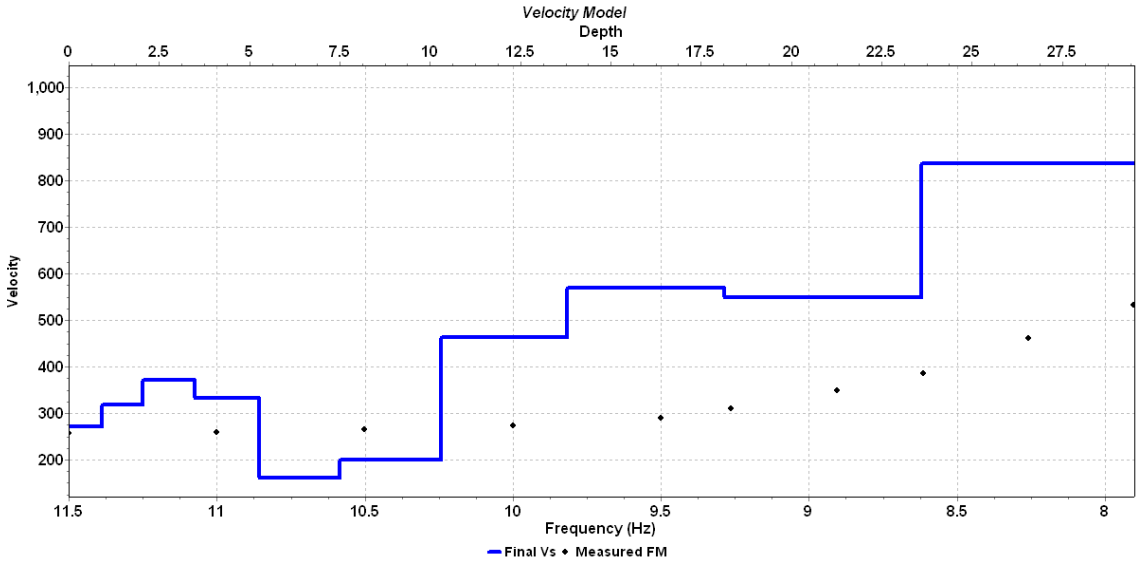

Figure 20: The fundamental-mode dispersion curve and shear wave velocity profile between Lachen and Thangu valley (MASW4)

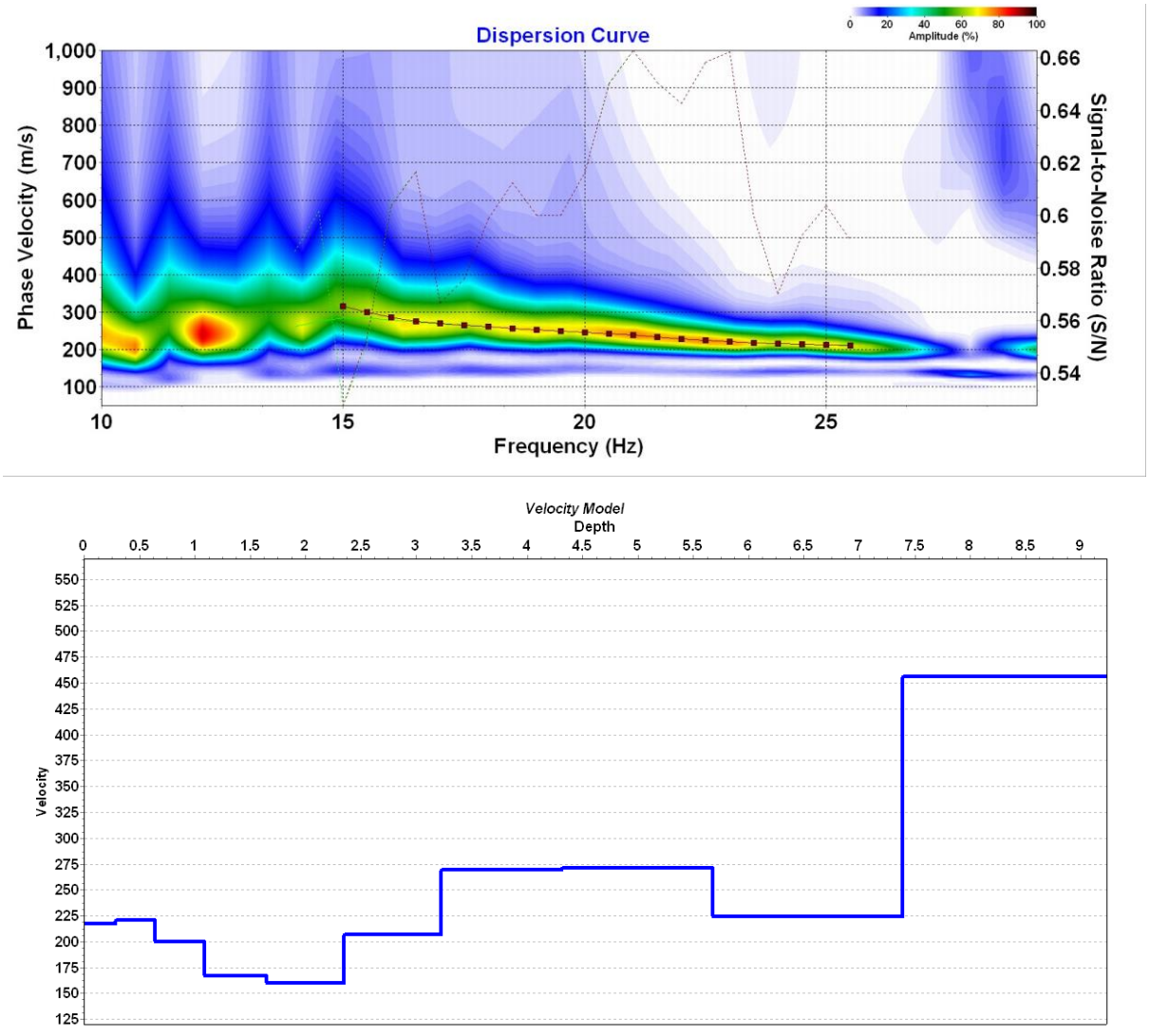

Figure 21: The fundamental-mode dispersion curve and shear wave velocity profile between Lachen and Thangu Valley (MASW5)

Analyzing the dispersion curves obtained for various locations and at different altitudes in North Sikkim shows that in the case of Lachung playground at an elevation of 2585 m a.s.l (MASW1), the frequency ranges between 20 Hz and 26 Hz, as shown in Figure 17. Figure 18 shows the dispersion curve for Changme glacial snout (MASW2) at an elevation of 4698 m a.s.l where the frequency lies in the range of 11 to 40 Hz. In Figure 19, the control points have a higher mode because of the modal jump in the dispersion curve between 14 to 23 Hz. Similarly, in Figures 20 and 21, the dispersion curve control points range between 8 to 11 Hz and 15 to 26 Hz, respectively.

4.3. Shear Wave Characterization of Soil/moraine/glaciofluvial Deposits

Several types of research have been conducted, and numerous methods have been proposed for the classification of rocks and soils based on their site-dependent amplification properties (Joyner et al. 1981; Tinsley et al. 1985; Borcherdt 1994; Will et al. 2000). Joyner et al. (1981) proposed a way to characterize site conditions using average shear wave velocities up to a depth equal to 0.25 times the wavelength of the dominant frequency. However, this method did not find extensive application due to execution difficulties. Borcherdt et al. (1991) developed a more simplified method using a correlation between the average shear wave velocity and amplification of ground motion up to 30m depth of rocks/sediments. This method has been incorporated into the National Earthquake Hazards Reduction Program (NEHRP). The NEHRP categorizes soils into different classes based on their thickness, vertical shear wave velocity profile, and liquefaction potential. According to NEHRP, the subsurface shear wave velocity (V_s) is estimated at up to 30m. The subsurface NEHRP V_s at a particular site can be calculated using eq. (4).

$$V_s = \frac{\sum_{i=1}^{n} D_i}{\sum_{i=1}^{n} \frac{D_i}{v_{si}}} \quad (4)$$

where V_s is the NEHRP shear wave velocity, D_i is the subsurface layer thickness (≤30m) and v_{si} is the shear wave velocity at the subsurface layer in m/s. Table 2 shows the NEHRP classification system.

Table 2: Classification of site soil profile type for seismic amplification (N: SPT blow count; S_u: Undrained shear strength; PI: Plasticity Index and w: Water content)

NEHRP site class	General description	Average V_s to 30m (m/s)
A	Hard rock	> 1500
B	Rock	760 < V_s ≤ 1500
C	Soft rock and very dense soil	360 < V_s ≤ 760
D	Stiff soil (50 kPa ≤ S_u ≤ 100 kPa or 15 ≤ N ≤ 50)	180 < V_s ≤ 360
E	Soil with more than 3m soft clay strata with PI ≥ 20, w ≥ 40%, and S_u < 25 kPa	≤ 180
F	Soils that need site-specific evaluations	

Analyzing the shear wave velocity (V_s) profiles for the five different locations in North Sikkim, the average V_s to 30m ($V_{s\,(30)}$) has been determined, as shown in Table 3. Maximum $V_{s\,(30)}$ has been observed at a location b/w Lachung and Thangu Valley (MASW4), which is about 537 m/s. This site can be classified as site class C, including Lachung Playground (MASW1), according to the NEHRP criteria. The Changme glacial snout region lying close to the high-altitude glaciated regions has the lowest $V_{s\,(30)}$ value (248 m/s) and NEHRP site class D has been assigned. All the other locations come under the NEHRP site class D, as shown in Table 3. Figure 22 shows the $V_{s\,(30)}$ interpolation map of the region generated using the inverse distance weighted (IDW) interpolation method.

Table 3: NEHRP site classification for the locations investigated in North Sikkim

(Code) Location	$V_{s\,(30)}$ (m/s)	NEHRP site class
(MASW1) Lachung Playground	394	C
(MASW2) Changme Glacial Snout	248	D
(MASW3) Yumthang Valley	321	D
(MASW4) b/w Lachen & Thangu Valley	537	C
(MASW5) b/w Lachen & Thangu Valley	296	D

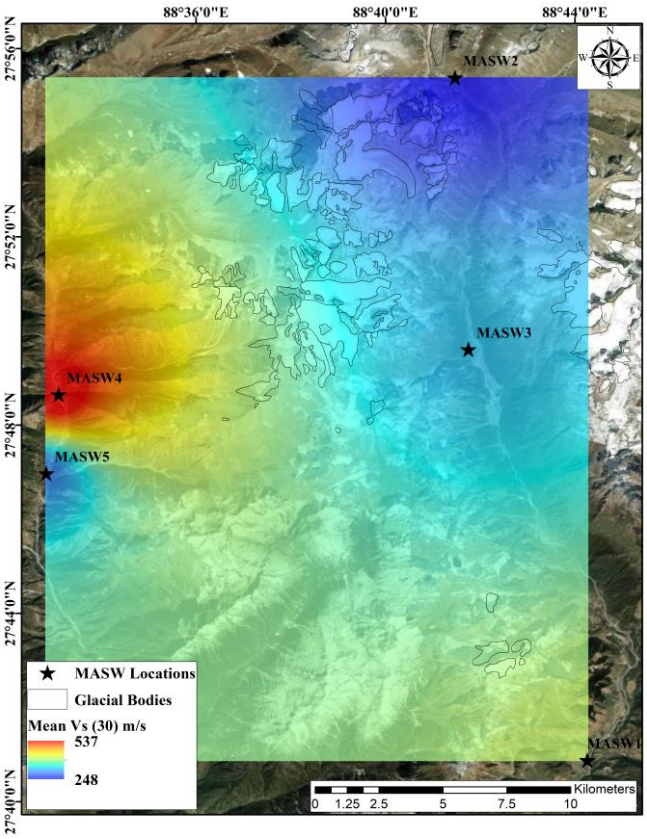

Figure 22: The $V_{s\,(30)}$ interpolation map of North Sikkim

4.4. GPR Survey in conjunction with MASW

The GPR survey has been performed in two locations (MASW5 & MASW2) in North Sikkim where the MASW survey has also been conducted, as shown in Figure 23. The subsurface profiling for the GPR survey has been executed for the same orientation as the MASW survey. For the location between Lachen and Thangu valley (MASW5), the GPR survey provided subsurface information up to the depth of 20m with three distinct layers of varying thickness. Demarcating the ground surface level at 0m, the initial layer extends up to 4m, followed by a second and third layer of about 4 and 12m thickness, respectively.

Figure 23: GPR survey at a location (MASW5) between Lachen and Thangu valley (left) and (MASW2) Changme glacial snout (right)

It is a well-understood fact that GPR imaging does not provide information regarding the sub-surface's index and/or mechanical properties. Therefore, the layers demarcated in this section are based purely on visual

inspection and interpretation of structural discontinuities underneath the ground surface. From 4 to 8m depth, observed parallel reflectors have been considered the basis of layer segregation. Within the 2nd layer extending up to 8m deep, a gentle slope from 5 to 6m has been observed, as shown in Figure 24 (left). However, it must be considered that GPR's imaging performance is hampered in clay-rich/conductive environments due to larger signal attenuation (Nath et al. 2018). Therefore, there exists the possibility that the tail of a diffraction hyperbolae is misinterpreted as a sloping layer. This problem has been solved from interpretation using both GPR and MASW results. The V_s profile of the same location and orientation has been obtained using the MASW setup as shown in Figure 21. V_s can be defined as the velocity at which shear waves generated due to an earthquake event will propagate through the subsurface strata of soil/rock. V_s is directly proportional to the subsurface material's shear modulus ($\bar{G}$), which is a dynamic geotechnical property. Therefore, the estimation of V_s for a subsurface stratum can be considered the firsthand step in assessing the local site condition as it represents the stiffness of different subsurface layers. An attempt to comprehend the results from MASW and GPR simultaneously has helped gather some interesting observations in this case. The GPR-based subsurface imaging indicates an inclined layer between 5 and 6m depth from the ground surface. The results obtained from the MASW survey reveal a fragile layer ($V_s \leq$ 275 m/s) up to 7.3m deep from the ground surface. A sudden drop in V_s at 6m depth has been observed that can be attributed to the existence of layer inclination at this depth. Moreover, a sudden fall in the V_s has been observed between 6 and 7.3m depths followed by a sudden rise in the shear wave velocity then after. Increased V_s indicates increased stiffness of the subsurface layer and vice versa. This indicates a third layer with greater stiffness than the second layer from 7.3m to 20m depths.

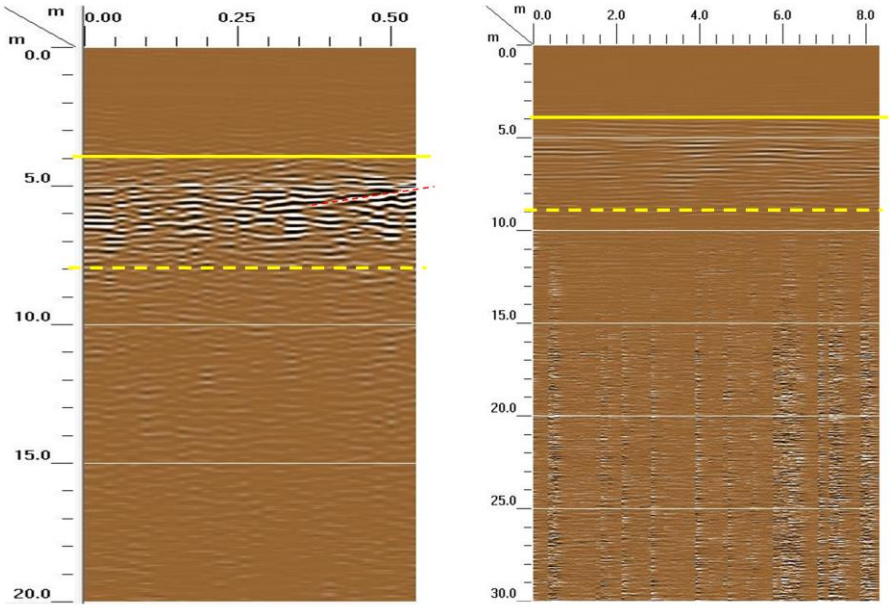

Figure 24: GPR results at two different locations (left: MASW5 & right: MASW2) in North Sikkim (continuous and dotted yellow lines denote the boundaries of the intermediate layer, and the dotted red line represents the inclined layer)

Figure 24 (right) shows the GPR survey at Changme glacial snout (MASW2). The results seem comparatively less informative than the MASW5 location. The first layer underneath the ground surface extends up to a depth of 4m, followed by a second layer of 5m thickness. Even though sets of parallel reflectors have been observed in the second layer, their visualization is less profound than the previous location (MASW5). The MASW survey shows a fragile layer up to 7.6m below the surface ($V_s \leq$ 300 m/s), as shown in Figure 18. However, V_s has been observed with an increase after 7.6m indicating a stiffer stratum underneath. Even though GPR profiling has helped in imaging the subsurface up to a depth of 30m, the information below 10m has been acquired with noise. This may be attributed to the dispersion and scattering of radio waves at that depth. As glacio-fluvial deposits characterize the location, GPR may not be sufficient to investigate the subsurface to much deeper strata.

4.5. Laboratory-based Geotechnical Testing

Geotechnical testing has been performed for the Changme glacial moraine (CM) and lacustrine (CL) samples and Rathong glacial moraine (RM) and lacustrine (RL) samples. The index properties, such as specific gravity, grain size distribution, and Atterberg's limits have been determined in accordance with the Indian Standard (IS) codal provisions mentioned in section 2.2 and Table 4. It has been observed that the specific gravity (G) of CM shows

close similitude with RM. Similarly, not much differences in the specific gravity have also been observed between the CL and RL samples. In the case of Changme glacial deposits, CM has been observed with the dominance of non-plastic silt (~70%) with some fine and medium sand with no clay. The glaciofluvial sample (CL) from the same location has been identified with the major composition of fine sand (~77%) with an appreciable amount of silt (~21%) and a trace amount of medium sand but devoid of clayey particles. The liquid limit (LL) for both CM and CL samples has been determined as 25.23% and 35.9%, respectively (Table 4). However, the plastic (PL) and shrinkage limits (SL) could not be determined for either of the samples due to the presence of non-plastic silt. The moraine sample (RM) obtained from the Rathong glacial snout has been observed with a large proportion of gravel (~40%) with a significant amount of sand (~60%). On the other hand, the RL sample has a dominance of fine and medium sand (~91%) with trace amounts of coarser sand particles and silt, as shown in Table 5. As also observed for CM and CL samples, the RM and RL samples lack clay. The Atterberg's limits for the Rathong samples have not been determined because the samples are composed of coarse-grained particles in abundance and finer particles such as silt and clay are either completely absent or present in negligible amounts. Thus, the moraine and glaciofluvial samples from the Rathong region have been classified as poorly graded sand (SP) as per the provisions of the IS code.

Table 4: Index properties of deposits from Changme glacial snout

Properties	Value		Standard
	Moraine	Lacustrine	
Specific Gravity	2.55	2.61	IS 2720 (Part III) - 1980
Grain Size Distribution (%)			
Coarse Sand (4.75-2 mm)	0.00	0.00	IS 2720 (Part IV) - 1985
Medium Sand (2-0.425 mm)	10.00	2.15	
Fine Sand (0.425-0.075 mm)	19.98	77.21	
Silt (0.075-0.002 mm)	70.02	20.64	
Clay (<0.0002 mm)	0.00	0.00	
Atterberg 's Limit (%)			
Liquid Limit (LL)	25.23	35.90	IS 2720 (Part V) - 1985
Plastic Limit (PL)	NA	NA	
Shrinkage Limit (SL)	NA	NA	IS 2720 (Part IV) - 1972

Table 5: Index properties of deposits from Rathong glacial snout

Properties	Value	
	Moraine	Lacustrine
Specific Gravity	2.54	2.58
Grain Size Distribution (%)		
Gravel (>4.75 mm)	40.40	0.00
Coarse Sand (4.75-2 mm)	10.45	4.51
Medium Sand (2-0.425 mm)	29.62	31.21
Fine Sand (0.425-0.075 mm)	19.53	59.45
Silt (0.075-0.002 mm)	0.00	4.83
Clay (<0.0002 mm)	0.00	0.00
Atterberg 's Limit (%)		
Liquid Limit (LL)	NA	NA
Plastic Limit (PL)	NA	NA
Shrinkage Limit (SL)	NA	NA
Soil Classification (IS)	SP	SP

Considering the grain size distribution of the samples, compaction properties have been determined for CM and CL and not for RM and RL as optimum moisture content (OMC) and maximum dry density (MDD) are not preferred for coarse-grained soil. The OMC and MDD values for CM and CL samples have been mentioned in Table 6. A direct shear test has been performed to determine the shear strength properties (cohesion (c) and angle of internal friction (ϕ)) of the samples. Owing to the larger amount of silt in the CM sample, a much higher value of cohesion (22.3 kPa) has been observed as compared to RM as shown in Table 7. However, the ϕ value is higher for RM. In the case of CL and RL samples, the shear strength properties (c and ϕ) do not show much variations. The coefficient of permeability (k), obtained from the constant head permeability test, lies in the range of 10^{-4} to 10^{-3} and 10^{-6} to 10^{-5} for Rathong and Changme samples, respectively. The maximum and minimum void ratios for RM and RL samples, as obtained from the relative density test, are shown in Table 7.

Table 6: Engineering properties of deposits from Changme glacial snout

Properties	**Value**		**Standard**
	Moraine	**Lacustrine**	
Compaction Properties			
Optimum Moisture Content (%)	14	19	IS 2720 (Part VII) - 1980
Maximum Dry Density (g/cc)	1.80	1.65	
Shear Strength Properties			
Cohesion (kPa)	22.30	14.83	IS 2720 (Part XIII) - 1986
Angle of Internal Friction (°)	15.61	19.54	
Coefficient of Permeability (k in cm/s)	10^{-6}-10^{-5}		IS 2720 (Part XVII) - 1986

Table 7: Engineering properties of deposits from Rathong glacial snout

Properties	**Value**		**Standard**
	Moraine	**Lacustrine**	
Shear Strength Properties			
Cohesion (kPa)	5.43	16.73	IS 2720 (Part XIII) - 1986
Angle of Internal Friction (°)	22.44	20.42	
Coefficient of Permeability (k in cm/s)	10^{-4} -10^{-3}		IS 2720 (Part XVII) - 1986
Maximum void ratio (e_{max})	0.48	0.87	
Minimum void ratio (e_{min})	0.22	0.43	IS 2720 (Part XIV) - 1983

The physiochemical and micro-structural analysis of the moraine and lacustrine samples have been performed at the Central Instrument Facility (CIF), Indian Institute of Technology Guwahati. The morphological structure of the sediments has been examined with the help of field emission scanning electron microscopy (FESEM) (Zeiss, Gemini 300, Germany). Also, the mineralogical composition of the samples has been examined using X-ray Diffraction (XRD) (Rigaku, SmartLab9KW, Japan). The instrument is equipped with D/tex ultra 250 solid-state detectors working at λ=1.54A and Cu-kα X-ray source. The samples have been scanned at 3° to 80° diffraction angles, the scan speed of 20° 2θ/min, and 0.02 step size. The mineralogical composition thus obtained has been confirmed using available literature and the International Center for Diffraction Data (ICDD).

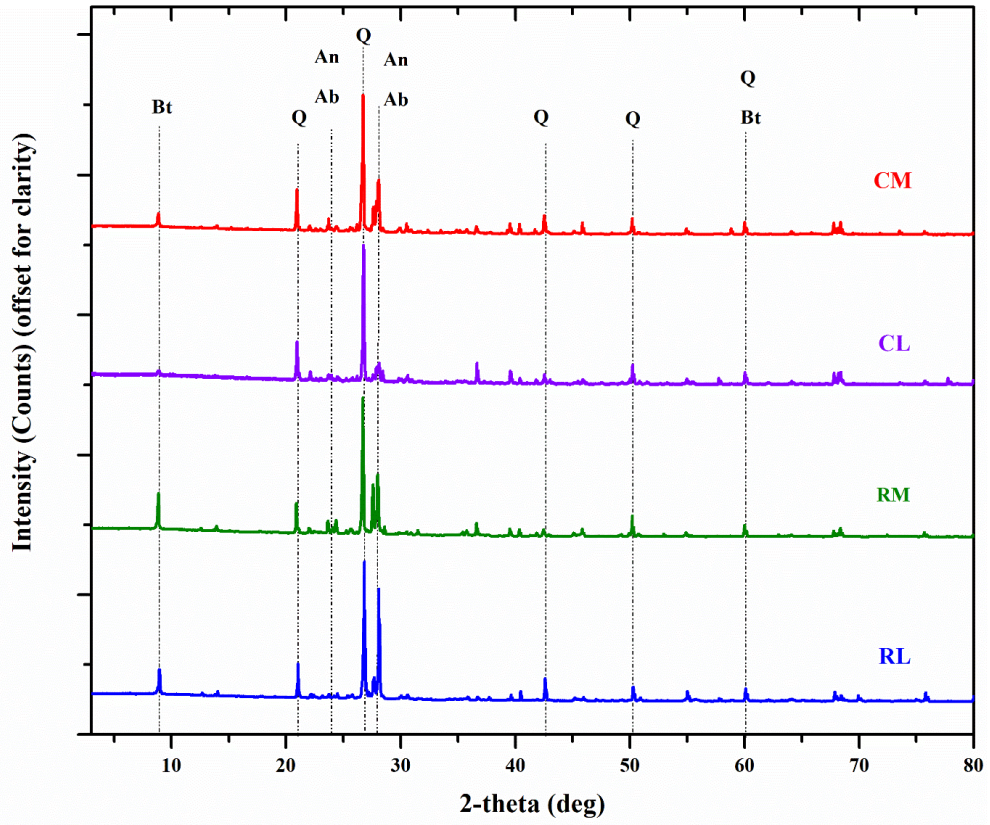

Figure 25: XRD pattern of moraine and lacustrine deposits from Changme and Rathong glacial snout (Bt: Biotite; Q: Quartz; Ab: Albite and An: Anorthite)

Figure 25 represents the XRD spectral analysis of the samples. Major minerals such as Quartz (Q: SiO_2), Biotite (Bt: $K(Mg, Fe)_3AlSi_3O_{10}(F, OH)_2$), Albite (Ab: $NaAlSi_3O_8$), and Anorthite (An: $CaAl_2Si_2O_8$) have been identified from the XRD diffractogram. Silica (Si) and oxygen (O) have been found as the most abundant elements in all the moraine and glaciofluvial deposition samples using energy dispersive X-ray (EDX). Apart from these two major elements, aluminum (Al) and iron (Fe) have been identified along with some alkali metals such as sodium (Na) and potassium (K) and some alkali earth metals such as calcium (Ca) and magnesium (Mg). The surface morphology of the sediments obtained from the Changme and Rathong glacial environments, has been shown in Figure 26.

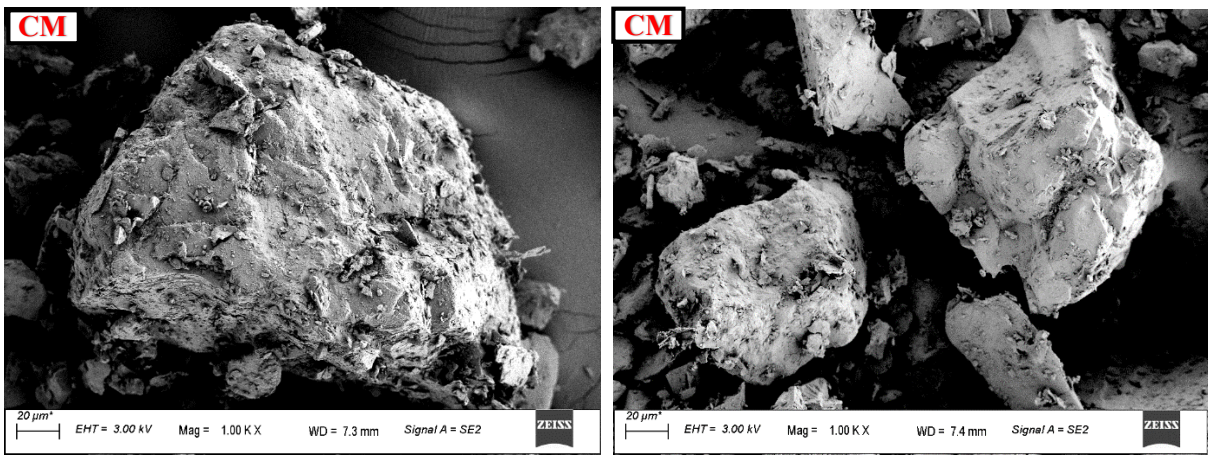

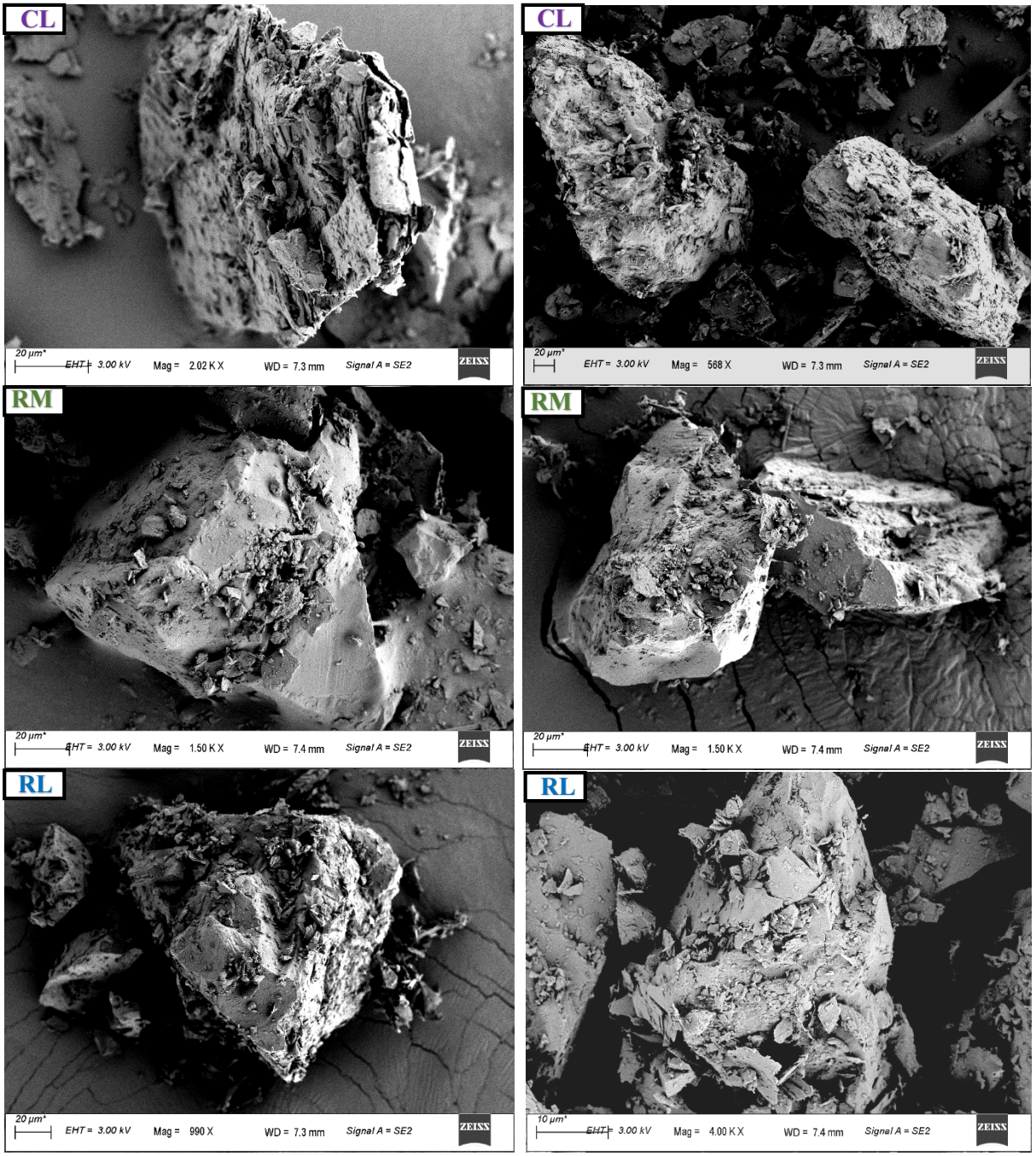

Figure 26: Surface morphology of Changme glacial moraine (CM), lacustrine deposits (CL), Rathong glacial moraine (RM) and lacustrine deposits (RL)

4.6. Stability Assessment of Moraine Slopes at Glacial Environment

Stability analysis of moraine slopes on either side of the Chagnme and Rathong glacial snout has been performed using LEM considering various cross-sections. Figure 27 shows that for cross-section-1 (C-1), the FoS of the left slope is 0.658 and less than the right slope (FoS = 0.959). As the material properties and boundary conditions remain the same for the assessment of slopes on both the sides of Changme glacial snout, the left slope, being steeper than the right slope, shows lesser FoS. The process of stability analysis is repeated for another three cross-sections (C-2/C-3/C-4), and similar observations have been made except for C-2, where the left and right slopes show almost the same FoS (0.66). Figure 28 shows the stability assessment of moraine slopes on either side of Rathong glacial snout. Similar to that of Changme moraine slopes, the FoS lies less than 1 indicating unstable slopes. The FoS remains close to 0.8 for moraine slopes along all the cross-sections at Rathong glacial snout. Site investigations corroborate these findings, revealing failed slope sections and frequent rockfalls in the vicinity of both glacial snouts. Also, some of the slopes were identified with underlying glacial calving zones. The presence of underlying glacial calving zones, which leave large portions of the slope base hollow, exacerbates the instability.

Continued calving in these areas increases the likelihood of catastrophic slope failure, underscoring the urgent need for monitoring and potential mitigation efforts to manage these geohazards.

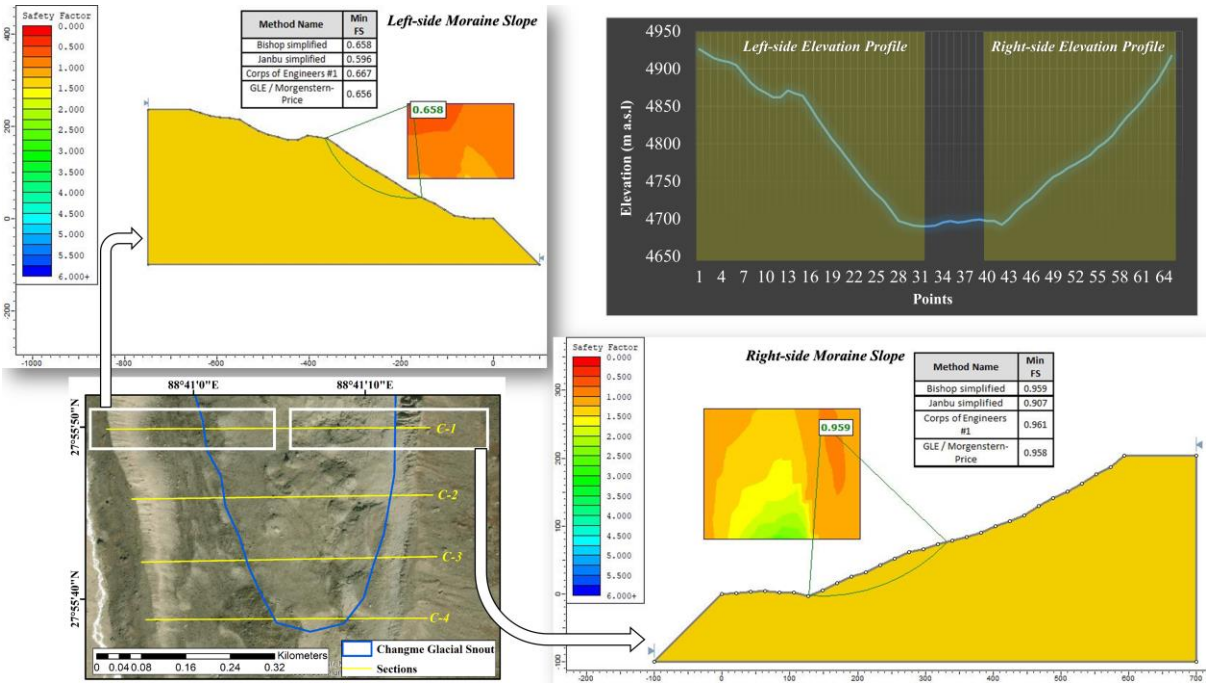

Figure 27: Limit equilibrium analysis of moraine slopes on either sides of Changme glacial snout

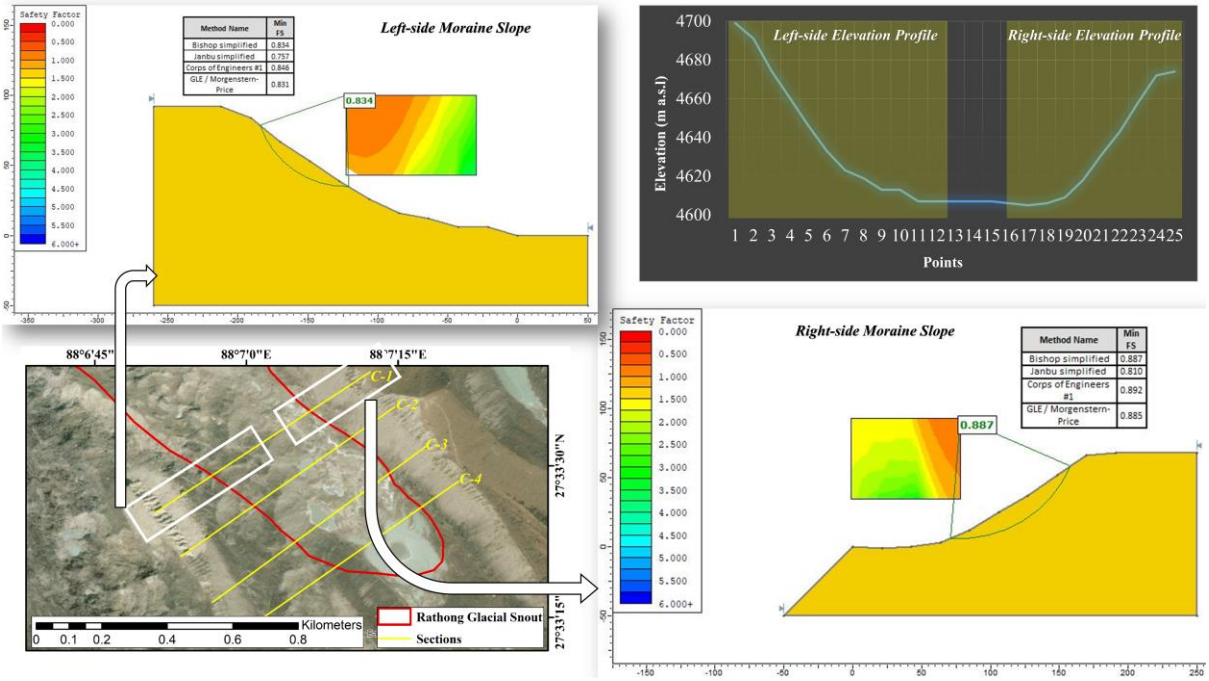

Figure 28: Limit equilibrium analysis of moraine slopes on either side of Rathong glacial snout

4.7. Recommendations for Critical Slopes

The goal of investigating the naturally deposited moraine slopes on either side of glacial snouts in the Sikkim Himalayas is to put a step forward towards stabilizing the moraine slopes, which act as embankments for proglacial lakes. In the event of slope failures, moraine material can generate waves that may lead to outburst floods. One such example is the failure of the lateral moraine wall of South Lhonak glacial lake and the outburst flood on 4th October 2023 (Yu et al. 2024; Mondal et al. 2024). This study is a state-of-the-art attempt to conduct a comprehensive investigation of these glacial deposits. The findings are valuable for calculating the factor of

safety (FoS) of moraine slopes that serve as embankments for various glacial lakes in Sikkim. Further, similar attempts can be made in other parts of the Hindu-Kush Himalayas as well.

This analysis adds a critical component to the risk assessment of glacial lakes concerning outburst floods, focusing on the stability of moraine embankments around these lakes. Key factors influencing stability are not just the hydrological and hydrodynamic parameters but also the material properties and geometry of embankments that govern the FoS. Understanding these factors using field- and satellite-based analysis will help pinpoint vulnerable areas in moraine embankments that need immediate attention.

Unlike soil and rock slopes, glacial moraine slopes in the high-altitude Himalayas are inherently unstable and fragmented. As a result, conventional methods such as trimming (gentling) through benching may not be effective. Field investigations reveal that these moraine slopes consist of a range of materials from fine sand and silt to large boulders, making them highly susceptible to rockfall. This instability means that disturbing the slopes with traditional engineering stabilization techniques could potentially trigger sliding and/or rockfall. One viable approach is to install flexible fences made of steel mesh along the slope to catch falling debris and/or cover vulnerable zones with wire mesh netting to prevent loose rocks from detaching and falling.

5. Conclusion

Debris and moraine cover on Himalayan glaciers not only alter the absorption of solar radiation, leading to increased glacial melting, but they can also serve as a protective layer for the ice beneath. These moraines, transported by glaciers, form slopes alongside the glacier and function as natural barriers for various glacial lakes. The failure of these slopes or natural embankments can sometimes lead to disasters, such as Glacial Lake Outburst Floods (GLOFs). The extensive geospatial, geophysical, and geotechnical analysis conducted in this study offers a thorough understanding of the glacial deposits in the Sikkim Himalayas. This knowledge is crucial for creating effective hazard mitigation strategies, particularly given the challenging conditions in the Himalayan region.

- Investigating the glacial bodies within Sikkim Himalayas revealed distinct patterns in albedo, glacial surface temperature (GST), debris cover, and backscatter responses, highlighting the impacts of glacial debris and moraine. As the albedo decreases towards the glacial snout due to increased debris cover, GST rises, indicating enhanced absorption of solar radiation and subsequent melting. This phenomenon is most pronounced in the glacier's lower reaches, where debris cover is extensive. The mapping of debris cover shows that the cleaner ice and snow are predominantly found at higher elevations, while the trunk and snout regions are heavily covered with debris, correlating with higher GST and lower albedo. The analysis of C-band backscatter data from recent years indicates a significant increase in the area and number of supraglacial lakes, reflecting a rise in glacial melt. These findings underscore the critical role of debris cover in influencing glacier melt dynamics and the formation of supraglacial lakes, with important implications for understanding and managing glacial hazards in the region.
- The field- and lab-based investigations conducted in North Sikkim have provided valuable insights into the subsurface and surface characteristics of these regions. Utilizing MASW and GPR, the study identified significant variations in shear wave velocity (V_s) profiles and subsurface stratigraphy. A site b/w Lachen and Thangu Valley, the highest average $V_{s\,(30)}$ was observed, indicating a relatively stiff subsurface layer classified as NEHRP site class C, while the Changme glacial snout exhibited the lowest $V_{s\,(30)}$, classified as site class D, suggesting a more fragile subsurface. The MASW and GPR data highlighted a layered subsurface structure, with varying stiffness and the presence of inclined layers. However, at greater depths, particularly at Changme, GPR results were less clear, likely due to the dispersion and scattering of radio waves in glacio-fluvial deposits. This study underscores the complexity of subsurface conditions in glacial environments and the limitations of GPR in deeper strata, emphasizing the need for complementary geophysical methods to better characterize these areas.
- The geotechnical and microstructural analysis of moraine and lacustrine samples from Changme and Rathong glaciers reveals key insights into their composition and properties. Both sites showed similar specific gravity in their moraine and lacustrine samples. The Changme moraine predominantly consists of non-plastic silt, while the lacustrine deposits contain mainly fine sand. The Rathong moraine is characterized by a significant gravel and sand content, with lacustrine deposits largely composed of sand. Due to the coarse-grained nature of the Rathong samples, Atterberg limits were not determined. Permeability tests indicated higher values for Rathong samples compared to Changme. The mineralogical analysis identified common minerals like quartz, biotite, albite, and anorthite, with silica and oxygen as the predominant elements, alongside trace amounts of aluminum, iron, sodium, potassium, calcium, and magnesium. FESEM analysis provided detailed insights into the sediment morphology, confirming the compositional findings.
- The stability analysis of moraine slopes at Changme and Rathong glacial snouts, conducted using the limit equilibrium method (LEM), indicates a consistent risk of instability, with Factors of Safety (FoS) less than 1

across various cross-sections. This instability is more pronounced on the steeper left slopes of the Changme snout and uniformly critical at Rathong, where FoS values approximate 0.8. Field investigations support these findings, revealing failed slopes, frequent rockfalls, and the presence of underlying glacial calving zones, further undermining slope stability. These conditions highlight the significant risk of catastrophic slope failure, emphasizing the need for continuous monitoring and the implementation of mitigation strategies to address these geohazards.

The investigation of moraine slopes in the Sikkim Himalayas highlights their critical role as natural embankments for proglacial lakes, where slope failure could trigger outburst floods, as evidenced by the South Lhonak glacial lake event on 4th October 2023. This study emphasizes the importance of understanding the factors influencing the stability of these moraine embankments, including material properties and geometric configurations. Given the inherent instability and heterogeneous composition of such glacial moraine slopes, conventional stabilization methods like benching might be impractical. Instead, the study suggests alternative measures, such as installing flexible fences and wire mesh netting to manage rockfall risks. These findings are crucial for enhancing the risk assessment and management of glacial lakes in the Sikkim Himalayas and can serve as a model for similar regions in the Hindu-Kush Himalayas.

Data availability. *Data will be made available upon request.*

Author contribution. Sandeep Kumar Mondal: Conceptualization, Methodology, Visualization, Writing – original draft. Hrik Chaudhury: Methodology. Deepali Anand: Methodology. Rishikesh Bharti: Conceptualization, Methodology, Writing – review & editing. Abhishek Kumar: Conceptualization, Methodology, Writing – review & editing. Arindam Dey: Conceptualization, Methodology, Writing – review & editing.

Competing interests. The authors declare that they have no known competing financial interests or personal relationships that could have appeared to influence the work reported in this paper..

Funding. Not Applicable

Acknowledgments. The authors express their gratitude to the National Remote Sensing Centre (NRSC) and the Indian Space Research Organization (ISRO), the United States Geological Survey (USGS), the European Space Agency (ESA), the Alaska Satellite Facility (ASF), and the Randolph Glacial Inventory (RGI) for providing the data used in this study. We also extend our sincere gratitude to the Defence Geoinformatics Research Establishment (DGRE), the state administration of the Government of Sikkim, and the Indian Army for their valuable support during the field investigation.

References

Abramson, L.W., Lee, T.S., Sharma, S. and Boyce, G.M., 2001. Slope stability and stabilization methods. John Wiley & Sons.

Aggarwal, S., Rai, S.C., Thakur, P.K. and Emmer, A., 2017. Inventory and recently increasing GLOF susceptibility of glacial lakes in Sikkim, Eastern Himalaya. Geomorphology, 295, pp.39-54. https://doi.org/10.1016/j.geomorph.2017.06.014

Agrawal, S., Raghavendra, S., Kumar, S. and Pande, H., 2019. Geospatial data for the himalayan region: requirements, availability, and challenges. Remote Sensing of Northwest Himalayan Ecosystems, pp.471-500. https://doi.org/10.1007/978-981-13-2128-3_22

Alifu, H., Johnson, B.A. and Tateishi, R., 2015. Delineation of debris-covered glaciers based on a combination of geomorphometric parameters and a TIR/NIR/SWIR band ratio. IEEE Journal of Selected Topics in Applied Earth Observations and Remote Sensing, 9(2), pp.781-792. https://doi.org/10.1109/JSTARS.2015.2500906

Balaban, C.I., Roberts, D.H., Evans, D.J. and Jamieson, S.S., 2024. Past glaciation of temperate-continental mountains: A model for a debris-charged plateau icefield/cirque glacier landsystem in the Southern Carpathians, Romania. Earth Surface Processes and Landforms, 49(2), pp.601-621. https://doi.org/10.1002/esp.5723

Bard, P.Y., 1995, August. Effects of surface geology on ground motion: recent results and remaining issues. In Proc. 10 European Conf. Earth. Eng., ed. Duma, Balkema, Rotterdam (pp. 305-323).

Begam, S., Sen, D. and Dey, S., 2018. Moraine dam breach and glacial lake outburst flood generation by physical and numerical models. Journal of hydrology, 563, pp.694-710. https://doi.org/10.1016/j.jhydrol.2018.06.038

Behera, P.K., Sarkar, K., Singh, A.K., Verma, A.K. and Singh, T.N., 2016. Dump slope stability analysis–a case study. Journal of the Geological Society of India, 88, pp.725-735. https://doi.org/10.1007/s12594-016-0540-4

Berthier, E., Arnaud, Y., Kumar, R., Ahmad, S., Wagnon, P. and Chevallier, P., 2007. Remote sensing estimates of glacier mass balances in the Himachal Pradesh (Western Himalaya, India). Remote Sensing of Environment, 108(3), pp.327-338. https://doi.org/10.1016/j.rse.2006.11.017

Berthier, E., Floriciou, D., Gardner, A.S., Gourmelen, N., Jakob, L., Paul, F., Treichler, D., Wouters, B., Belart, J.M., Dehecq, A. and Dussaillant, I., 2023. Measuring glacier mass changes from space—a review. Reports on Progress in Physics, 86(3), p.036801. https://doi.org/10.1088/1361-6633/acaf8e

Bhambri, R. and Bolch, T., 2009. Glacier mapping: a review with special reference to the Indian Himalayas. Progress in Physical Geography, 33(5), pp.672-704. https://doi.org/10.1177/0309133309348112

Bolibar, J., Rabatel, A., Gouttevin, I., Zekollari, H. and Galiez, C., 2022. Nonlinear sensitivity of glacier mass balance to future climate change unveiled by deep learning. Nature communications, 13(1), p.409.

Bozhinskiy, A.N., Krass, M.S. and Popovnin, V.V., 1986. Role of debris cover in the thermal physics of glaciers. Journal of Glaciology, 32(111), pp.255-266.

Cassidy, W., Harvey, R., Schutt, J., Delisle, G. and Yanai, K., 1992. The meteorite collection sites of Antarctica. Meteoritics, 27(5), pp.490-525.

Cheng, Y.M., Lansivaara, T. and Wei, W.B., 2007. Two-dimensional slope stability analysis by limit equilibrium and strength reduction methods. Computers and geotechnics, 34(3), pp.137-150.

Clarke, B.G., 2017. Engineering of glacial deposits. CRC Press.

Claverie, M., Ju, J., Masek, J.G., Dungan, J.L., Vermote, E.F., Roger, J.C., Skakun, S.V. and Justice, C., 2018. The Harmonized Landsat and Sentinel-2 surface reflectance data set. Remote sensing of environment, 219, pp.145-161.

Corripio, J., Purves, R. and Rivera, A., 2007. Modeling climate-change impacts on mountain glaciers and water resources in the Central Dry Andes. Darkening Peaks: Glacier Retreat, Science and Society, pp.126-135.

Dashora, A., Lohani, B. and Malik, J.N., 2007. A repository of earth resource information–CORONA satellite programme. Current Science, pp.926-932.

Donahue, C.P., Menounos, B., Viner, N., Skiles, S.M., Beffort, S., Denouden, T., Arriola, S.G., White, R. and Heathfield, D., 2023. Bridging the gap between airborne and spaceborne imaging spectroscopy for mountain glacier surface property retrievals. Remote Sensing of Environment, 299, p.113849.

Dubey, J., Ali, S.N., Sharma, A., Morthekai, P., Singh, R., Sharma, R.K., Pandey, P., Thakur, B. and Srivastava, V., 2019. Glacial geomorphology and landscape evolution of the Thangu valley, North Sikkim Himalaya, India. Journal of the Indian Society of Remote Sensing, 47, pp.821-837.

Evans, D.J., 2016. Landscapes at the periphery of glacierization–retrospect and prospect. Scottish Geographical Journal, 132(2), pp.140-163.

Fredin, O., Bergstrøm, B., Eilertsen, R., Hansen, L., Longva, O., Nesje, A. and Sveian, H., 2013. Glacial landforms and Quaternary landscape development in Norway. Quaternary Geology of Norway, edited by: Olsen, L., Fredin, O., and Olesen, O., Geological Survey of Norway Special Publication, Geological Survey of Norway, Trondheim, 525.

Garg, P.K., Shukla, A. and Jasrotia, A.S., 2019. On the strongly imbalanced state of glaciers in the Sikkim, eastern Himalaya, India. Science of the Total Environment, 691, pp.16-35.

Garg, S., Shukla, A., Mehta, M.A.N.I.S.H., Kumar, V.I.N.I.T. and Shukla, U.K., 2019. On geomorphic manifestations and glaciation history of the Kangriz glacier, western Himalaya. Himal. Geol, 40(2), pp.115-127.

Gomez, M.L., Hoke, G., D'Ambrosio, S., Moreiras, S. and Castro, A., 2022. Hydrogeology of Northern Mendoza (Argentina), from the Andes to the eastern plains, in the context of climate change. Hydrogeology Journal, 30(3), pp.725-750.

Google Earth Engine, 2022. A planetary-scale platform for Earth science data & analysis.

Gulácsi, A. and Kovács, F., 2020. Sentinel-1-imagery-based high-resolution water cover detection on wetlands, Aided by Google Earth Engine. Remote Sensing, 12(10), p.1614.

Hauck, C. and Mühll, D.V., 2003. Inversion and interpretation of two-dimensional geoelectrical measurements for detecting permafrost in mountainous regions. Permafrost and periglacial processes, 14(4), pp.305-318.

Herman, F., De Doncker, F., Delaney, I., Prasicek, G. and Koppes, M., 2021. The impact of glaciers on mountain erosion. Nature Reviews Earth & Environment, 2(6), pp.422-435.

Hird, J.N., DeLancey, E.R., McDermid, G.J. and Kariyeva, J., 2017. Google Earth Engine, open-access satellite data, and machine learning in support of large-area probabilistic wetland mapping. Remote sensing, 9(12), p.1315.

Hoover, R.B. and Gilichinsky, D., 2001. Significance to astrobiology of micro-organisms in permafrost and ice. In Permafrost response on economic development, environmental security and natural resources (pp. 553-579). Dordrecht: Springer Netherlands.

Huo, D., Bishop, M.P. and Bush, A.B., 2021. Understanding complex debris-covered glaciers: Concepts, issues, and research directions. Frontiers in Earth Science, 9, p.652279.

IS: 2720 (Part 6), 1972. Methods of test for soils: determination of shrinkage factors. Reaffirmed 2001.

IS: 2720 Part 17 (1986) Methods of Test for Soils: Laboratory Determination of Permeability (second revision). New Delhi: Bureau of Indian Standards.

IS: 2720 Part 3, 1980. Methods of Test for Soils–Determination of Specific Gravity.

IS: 2720 Part 5 (1985) Determination of Liquid Limit and Plastic Limit of Soil. New Delhi: Bureau of Indian Standards.

IS: 2720, Part–13, 1986. Methods of test for soils: direct shear test.

IS: 2720-Part 4. "Methods of test for soils: grain size analysis." (1985).

Israil, M. and Pachauri, A.K., 2003. Geophysical characterization of a landslide site in the Himalayan foothill region. Journal of Asian Earth Sciences, 22(3), pp.253-263.

Lee, J.S., 1981. Refined filtering of image noise using local statistics. Computer graphics and image processing, 15(4), pp.380-389.

Li, H., Harvey, J. and Kendall, A., 2013. Field measurement of albedo for different land cover materials and effects on thermal performance. Building and environment, 59, pp.536-546.

Liang, S., 2001. Narrowband to broadband conversions of land surface albedo I: Algorithms. Remote sensing of environment, 76(2), pp.213-238.

Liao, H., Liu, Q., Zhong, Y. and Lu, X., 2020. Landsat-based estimation of the glacier surface temperature of Hailuogou glacier, Southeastern Tibetan Plateau, between 1990 and 2018. Remote Sensing, 12(13), p.2105.

Mondal, S.K. and Bharti, R., 2021, July. Smoulder Detection Using Split-Window Algorithm: A Case Study From Baghjan Oilfield, Assam, India. In 2021 IEEE International Geoscience and Remote Sensing Symposium IGARSS (pp. 8590-8593). IEEE.

Mondal, S.K. and Bharti, R., 2022a. Glacial burst triggered by triangular wedge collapse: a study from Trisul Mountain near Ronti glacier valley. Geomatics, Natural Hazards and Risk, 13(1), pp.830-853.

Mondal, S.K., Das, A., Baba, R.H., Patel, V.D. and Bharti, R., 2024, July. Investigation of Glacial Lakes in Proximity to Failed South Lhonak Lake: A Glacio-Centric Approach to Disaster Risk Assessment. In IGARSS 2024-2024 IEEE International Geoscience and Remote Sensing Symposium (pp. 1904-1907). IEEE.

Mondal, S.K., Bharti, R. and Tiampo, K.F., 2023b. Seismic Deformation of Himalayan Glaciers Using Synthetic Aperture Radar Interferometry. EGUsphere, 2023, pp.1-37.

Nath, R.R. and Jakka, R.S., 2012, September. Effect of bedrock depth on site classification. In 15th world conference on earthquake engineering 15WCEE. Lisbon, Portugal (pp. 24-28).

Nath, R.R., Kumar, G., Sharma, M.L. and Gupta, S.C., 2018. Estimation of bedrock depth for a part of Garhwal Himalayas using two different geophysical techniques. Geoscience Letters, 5, pp.1-9.

Nath, S.K. and Thingbaijam, K.K.S., 2012. Probabilistic seismic hazard assessment of India. Seismological Research Letters, 83(1), pp.135-149.

Nath, S.K., Adhikari, M.D., Devaraj, N. and Maiti, S.K., 2015. Seismic vulnerability and risk assessment of Kolkata City, India. Natural Hazards and Earth System Sciences, 15(6), pp.1103-1121.

Nath, S.K., Srivastava, N., Ghatak, C., Adhikari, M.D., Ghosh, A. and Sinha Ray, S.P., 2018. Earthquake induced liquefaction hazard, probability and risk assessment in the city of Kolkata, India: its historical perspective and deterministic scenario. Journal of Seismology, 22, pp.35-68.

Nicholson, L., 2005. Modelling melt beneath supraglacial debris: implications for the climatic response of debris-covered glaciers. University of St. Andrews (United Kingdom).

Paul, F., Rastner, P., Azzoni, R.S., Diolaiuti, G., Fugazza, D., Le Bris, R., Nemec, J., Rabatel, A., Ramusovic, M., Schwaizer, G. and Smiraglia, C., 2019. Glacier inventory of the Alps from Sentinel-2, shape files. Supplement to: Paul, F, pp.1805-1821.

Pazzi, V., Morelli, S. and Fanti, R., 2019. A review of the advantages and limitations of geophysical investigations in landslide studies. International Journal of Geophysics, 2019.

Pilecki, Z., Isakow, Z., Czarny, R., Pilecka, E., Harba, P. and Barnaś, M., 2017. Capabilities of seismic and georadar 2D/3D imaging of shallow subsurface of transport route using the Seismobile system. Journal of Applied Geophysics, 143, pp.31-41.

Racoviteanu, A.E., Nicholson, L., Glasser, N.F., Miles, E., Harrison, S. and Reynolds, J.M., 2022. Debris-covered glacier systems and associated glacial lake outburst flood hazards: challenges and prospects. Journal of the Geological Society, 179(3), pp.jgs2021-084.

Raina, V.K. and Srivastava, D., 2021. Glacier atlas of India. GSI Publications, 7(1).

Raj, K.B.G., Remya, S.N. and Kumar, K.V., 2013. Remote sensing-based hazard assessment of glacial lakes in Sikkim Himalaya. Current Science, pp.359-364.

Sana, H. and Nath, S.K., 2017. Seismic source zoning and maximum credible earthquake prognosis of the Greater Kashmir Territory, NW Himalaya. Journal of Seismology, 21, pp.411-424.

Sass, O., 2007. Bedrock detection and talus thickness assessment in the European Alps using geophysical methods. Journal of Applied Geophysics, 62(3), pp.254-269.

Scherler, D., Bookhagen, B. and Strecker, M.R., 2011. Spatially variable response of Himalayan glaciers to climate change affected by debris cover. Nature geoscience, 4(3), pp.156-159.

Schrott, L. and Sass, O., 2008. Application of field geophysics in geomorphology: advances and limitations exemplified by case studies. Geomorphology, 93(1-2), pp.55-73.

Shrestha, A.B. and Aryal, R., 2011. Climate change in Nepal and its impact on Himalayan glaciers. Regional environmental change, 11, pp.65-77.

Shrivastava, P.K., Singh, G., Thapa, S.J., Chunchekar, R., Srivastava, H.B. and Mugal, V.V., 2022. Late Quaternary geomorphic evolution of Teesta-Khangtse basin, north Sikkim. Polar Science, 34, p.100868.

Shukla, T., Kumar, V. and Mehta, M., 2019. Response of the Himalayan glacial cycles to multiple equilibrium of climate system: a review. Quaternary international, 507, pp.4-14.

Singh, A., Kumar, R., Kumar, R., Singh, K.K. and Randhawa, S.S., 2022. Quantification of volume loss and snout retreat from 1980 to 2019 of baspa basin glaciers, western himalaya. Materials Today: Proceedings, 49, pp.3331-3339.

Singh, A.K., Kumar, D., Dubey, C.A., Gautam, P.K., Vishawakarma, B. and Singh, D.S., 2022. Glacial morpho-sedimentology and processes of landscape evolution in gangotri glacier area, Garhwal Himalaya, India. In Climate Change and Geodynamics in Polar Regions (pp. 223-238). CRC Press.

Singh, A.K., Kundu, J. and Sarkar, K., 2018. Stability analysis of a recurring soil slope failure along NH-5, Himachal Himalaya, India. Natural Hazards, 90, pp.863-885.

Snehmani, Singh, M.K., Gupta, R.D., Bhardwaj, A. and Joshi, P.K., 2015. Remote sensing of mountain snow using active microwave sensors: a review. Geocarto International, 30(1), pp.1-27.

Tanniru, S. and Ramsankaran, R.A.A.J., 2023. Passive microwave remote sensing of snow depth: Techniques, challenges and future directions. Remote Sensing, 15(4), p.1052.

Traversa, G., Fugazza, D., Senese, A. and Frezzotti, M., 2021. Landsat 8 OLI broadband albedo validation in Antarctica and Greenland. Remote Sensing, 13(4), p.799.

Veettil, B.K. and Kamp, U., 2017. Remote sensing of glaciers in the tropical Andes: a review. International journal of remote sensing, 38(23), pp.7101-7137.

Verma, A.K., Garg, P.K. and Hari Prasad, K.S., 2017. Sugarcane crop identification from LISS IV data using ISODATA, MLC, and indices based decision tree approach. Arabian Journal of Geosciences, 10, pp.1-17.

Weiß, T., 2018. sar-pre-processing Documentation. Prieiga internetu: https://buildmedia. readthedocs. org/media/pdf/multiply-sar-pre-rocessing/get_to_version_0, 4.

Yu, Y., Li, B., Li, Y. and Jiang, W., 2024. Retrospective Analysis of Glacial Lake Outburst Flood (GLOF) Using AI Earth InSAR and Optical Images: A Case Study of South Lhonak Lake, Sikkim. Remote Sensing, 16(13), p.2307.

Zhang, T., Wang, W. and An, B., 2024. A massive lateral moraine collapse triggered the 2023 South Lhonak Lake outburst flood, Sikkim Himalayas. Landslides, pp.1-13.